INTERNATIONAL JOURNAL FOR NUMERICAL METHODS IN FLUIDS, VOL. 25, 21–49 (1997)

ANALYSIS AND IMPLEMENTATION OF THE GAS-KINETIC BGK SCHEME FOR COMPUTATIONAL GAS DYNAMICS

CHONGAM KIM*, KUN XU, LUIGI MARTINELLI AND ANTONY JAMESON

Department of Mechanical and Aerospace Engineering, Princeton University, Princeton, NJ 08544, U.S.A.

SUMMARY

Gas-kinetic schemes based on the BGK model are proposed as an alternative evolution model which can cure some of the limitations of current Riemann solvers. To analyse the schemes, simple advection equations are reconstructed and solved using the gas-kinetic BGK model. Results for gas-dynamic application are also presented. The final flux function derived in this model is a combination of a gas-kinetic Lax–Wendroff flux of viscous advection equations and kinetic flux vector splitting. These two basic schemes are coupled through a non-linear gas evolution process and it is found that this process always satisfies the entropy condition. Within the framework of the LED (local extremum diminishing) principle that local maxima should not increase and local minima should not decrease in interpolating physical quantities, several standard limiters are adopted to obtain initial interpolations so as to get higher-order BGK schemes. Comparisons for well-known test cases indicate that the gas-kinetic BGK scheme is a promising approach in the design of numerical schemes for hyperbolic conservation laws. © 1997 by John Wiley & Sons, Ltd.

Int. J. Numer. Meth. Fluids, **25**: 21–49 (1997).

No. of Figures: 27. No. of Tables: 0. No. of References: 37.

KEY WORDS: gas evolution model; gas-kinetic BGK schemes; entropy condition; gas-kinetic Lax–Wendroff flux; kinetic flux vector splitting; local extremum diminishing; advection equations; non-linear hyperbolic systems

1. INTRODUCTION

Over the past few decades many numerical schemes for conservation laws have been proposed to solve gas-dynamic problems. One of the challenges is the clean capture of discontinuities such as shock waves and contact discontinuities while maintaining high accuracy in smooth flows including expansion regions. Upstream differencing or central differencing with suitable forms of artificial dissipation is generally used to compute the numerical flux at a cell boundary.

The design process of current shock-capturing schemes usually consists of two stages: an interpolation stage and a gas evolution stage based on the initial interpolated data. A clear physical picture of a numerical scheme can be found by examining these two stages.

In the interpolation stage, gas-dynamic quantities should be estimated at a cell boundary from discrete numerical data as accurately as possible. Remarkable progress has been made during the past two decades in this area. FCT (flux-corrected transport),[1,2] TVD (total variation diminishing),[3] MUSCL (monotonic upwind-centred schemes for conservation laws),[4,5] ENO (essentially non-oscillation),[6,7] PPM (piecewise parabolic method)[8,9] and LED (local extremum diminishing)[10,11]

*Correspondence to C. Kim, Department of Mechanical and Aerospace Engineering, Princeton University, Princeton, NJ 08544, U.S.A.

CCC 0271–2091/97/010021–29 $17.50

Received 11 January 1995
Revised 22 July 1996

schemes are the most noticeable advances. All these schemes exclude unphysical maxima or minima by introducing some kind of non-linear limiting process in constructing numerical data at a cell boundary. This essentially makes each scheme first-order-accurate near discontinuities. This constraint is generally referred to as the monotonicity condition and is consistent with Godunov's result that for a linear problem any oscillation-free scheme cannot be better than first-order-accurate across discontinuities.[12]

In the evolution stage a dynamic model of gas evolution based on the initial interpolated data is applied to find a numerical flux at an advanced time step. The accuracy and robustness of a numerical scheme depends on how realistically the dynamic model and interpolation principles can mimic the evolution of a real physical flow. Most of the modern high-resolution schemes use approximate or exact Riemann solvers as the evolution model.[13–15] Generally speaking, a Riemann solver assumes constant left and right states. As observed by van Leer,[16] if one uses a Riemann solver, a higher-order scheme is obtained by introducing a higher-order interpolation subject to the monotonicity condition. In this approach, higher-order slopes of gas-dynamic quantities are neglected after the left and right states are obtained at a cell boundary. A gas-dynamic quantity, however, is generally changing within a cell and this effect should be reflected in the gas evolution model. In this sense a Riemann solver can be interpreted as a first-order gas evolution model for a real physical flow. One of the issues in the present work is to improve this situation and to suggest a more physical gas evolution model while utilizing current interpolation principles.

The BGK (Bhatnager–Gross–Krook) model from gas-kinetic theory describes the multidimensional relaxation process of gas evolution from an initial non-equilibrium state to a final equilibrium state through particle collisions.[17] From the BGK model the time-dependent particle distribution function at a cell interface is obtained, from which the numerical fluxes are evaluated. In the BGK model any kind of higher-order local slope can be essentially incorporated and upstream differencing is achieved at the level of a particle motion. More notably, the entropy condition which is needed to prevent unphysical discontinuities becomes naturally satisfied. The intrinsic random motion of a gas particle provides a new possibility to obtain a multidimensional scheme without an appropriate wave modelling which is a crucial step in current multidimensional upwind schemes.[18,19] The BGK collisional model is different from the collisionless Boltzmann model which most Boltzmann-type schemes have adopted.[20–22] The collisionless Boltzmann model does not account for the gas relaxation process through particle collisions. Therefore the particle distribution function in a discontinuous region produces a large viscosity or heat conductivity due to two different half-Maxwellian distributions constructed from the left and right states of a cell boundary. This situation should be avoided for viscous or high-speed inviscid flow computations.

Recently the successful numerical implementation of the BGK model in various fluid dynamic problems has indicated the very promising behaviour of the BGK model as an alternative evolution model for computational gas dynamics.[23–26] Therefore it is necessary to characterize numerical and physical errors in the BGK flux function clearly and to find the relation of the BGK flux to other well-established numerical schemes. This path is somewhat similar to the one taken in the development of the Godunov scheme which is now recognized as an upwind scheme for gas-dynamic systems. The previous works,[23,24] however, did not address this issue. Recently it has been found that the BGK flux reduces either to the one-step Lax–Wendroff scheme or to the first-order flux vector splitting as the collision time (τ) of the BGK model approaches two extreme limits of zero or infinity.[25] To clarify this interpretation, both a linear advection equation and the Burgers equation are reconstructed from the BGK model and the algorithmic structure of the corresponding gas-kinetic schemes is analysed. Advection equations provide simple models which represent the formation or propagation of linear and non-linear waves, e.g. shock waves and contact discontinuities. Also, numerical results for different initial conditions give quantitative information on the behaviour of the scheme in various

flow conditions. Each term in the final BGK flux function has a definite physical or numerical interpretation. The final BGK flux has been identified as a non-linear combination of the two limiting schemes which represent the gas-kinetic Lax–Wendroff flux and kinetic flux vector splitting. A simplified BGK scheme which keeps important features of the original BGK scheme is also proposed. Finally, numerical comparisons of well-known test cases for gas-dynamic systems as well as advection equations are made to show that a scheme based on the BGK model is a promising approach in the design of numerical schemes for hyperbolic conservation laws.

2. GAS-KINETIC RECONSTRUCTION OF ADVECTION EQUATIONS

In gas-kinetic theory it is assumed that the mascroscopic fluid flow results from the collective motion of a large number of molecules. The complete description of a particle motion is given by the evolution equation of a particle distribution function $f(\vec{x}, t, \vec{u})$, where $\vec{x}$ is a space variable vector, t is a time variable and $\vec{u}$ is a particle velocity vector in phase space. From gas-kinetic theory, every macroscopic variable can be determined by the moments of a single scalar distribution function $f(\vec{x}, t, \vec{u})$. This provides a unified numerical approach from a scalar conservation law to systems of equations.

2.1. Analysis of the BGK model

For an advection equation with a mass variable U

$$U_t + a(U)U_x = 0, \tag{1}$$

where $a(U)$ is a local wave speed, the relation between the macroscopic variable U and the distribution function f is given by the moment

$$U(x, t) = \int_{-\infty}^{\infty} f(x, t, u)\mathrm{d}u. \tag{2}$$

The time evolution of f in three dimensions can be properly described by the Boltzmann equation

$$\frac{\mathrm{d}f}{\mathrm{d}t} = \frac{\partial f}{\partial t} + u\frac{\partial f}{\partial x} + v\frac{\partial f}{\partial y} + w\frac{\partial f}{\partial z} = C(f),$$

where u, v, w is a particle velocity in the x-, y-, z-direction and $C(f)$ represents a collision integral. The difficulty in solving the full Boltzmann equation lies in the non-linear integral property of the collision term $C(f)$. To overcome this problem, Bhatnager *et al.* have proposed an approximate collisional model.[17] In the one-dimensional case the evolution of f is expressed as

$$\frac{\partial f}{\partial t} + u\frac{\partial f}{\partial x} = C(f) \approx \frac{g - f}{\tau}. \tag{3}$$

Equation (3) describes the gas relaxation process in which an initial distribution function $f(x, t, u)$ approaches an equilibrium distribution function $g(x, t, u)$ over a collision time scale τ. Because we do not have additional equations for momentum and energy, only the mass conservation constraint is applied. From the conservation requirement that the integration of g and f with respect to the particle velocity should represent the same macroscopic variable U, the *compatibility condition* is obtained:

$$U = \int_{-\infty}^{\infty} f\,\mathrm{d}u = \int_{-\infty}^{\infty} g\mathrm{d}u \tag{4}$$

for all x, t.

Now we may examine how the BGK model describes the macroscopic flow. In a smooth region it is reasonable to assume that the flow is in a local thermodynamic equilibrium state. Hereafter an equilibrium state means a local thermodynamic equilibrium state. Thus we may assume that the

equilibrium distribution function is a Maxwellian distribution $g = Ae^{-\lambda[u-b(U)]^2}$, where λ determines the dispersion of the particle distribution function around an average macroscopic velocity, which will be discussed more in Section 3, and $b(U)$ is the macroscopic velocity to be determined. From equations (2) and (4) one obtains

$$g(x, t, u) = \sqrt{\left(\frac{\lambda}{\pi}\right)} U e^{-\lambda[u-b(U)]^2}.$$

If f remains in an equilibrium state with $f = g$, the BGK model gives

$$\frac{\partial g}{\partial t} + u\frac{\partial g}{\partial x} = 0. \tag{5}$$

Integrating the above equation with respect to the particle velocity in phase space (see Appendix I), we get

$$\int_{-\infty}^{\infty} (g_t + ug_x)\mathrm{d}u = \langle u^0, g\rangle_t + \langle u, g\rangle_x = U_t + [b(U)U]_x = 0, \tag{6}$$

where $\langle u^n, g\rangle \equiv \int_{-\infty}^{\infty} u^n g \mathrm{d}u$. As a special case of equation (1), a linear advection equation ($a(U) = c$) and the Burgers equation ($a(U) = U$) will be considered. From equation (6), $b(U) = a(U) = c$ for a linear advection equation and $b(U) = a(U)/2 = U/2$ for the Burgers equation can be used to recover each equation in a smooth region. At the same time the Maxwellian distribution for each equation is totally determined.

In a physically dissipative region the flow is in a non-equilibrium state. The behaviour of f can be quantitatively examined using the Chapman–Enskog expansion. The departure of f from an equilibrium state can be obtained from equation (3) up to the first order of τ (see Appendix II):

$$f \approx g - \tau(g_t + ug_x). \tag{7}$$

Equations (3) and (4) give

$$\int_{-\infty}^{\infty} \left(\frac{\partial f}{\partial t} + u\frac{\partial f}{\partial x}\right)\mathrm{d}u = \frac{1}{\tau}\int_{-\infty}^{\infty} (g - f)\mathrm{d}u = 0. \tag{8}$$

Substituting equation (7) into equation (8), we get

$$\int_{-\infty}^{\infty} (g_t + ug_x)\mathrm{d}u = \tau\frac{\partial}{\partial x}\int_{-\infty}^{\infty} u(g_t + ug_x)\mathrm{d}u$$

or

$$\langle u^0, g\rangle_t + \langle u, g\rangle_x = \tau(\langle u, g\rangle_t + \langle u^2, g\rangle_x)_x. \tag{9}$$

By using the recurrence relation of $\langle u^n, g\rangle$ (see Appendix I), for a linear advection equation, equation (9) becomes

$$U_t + cU_x = \tau\left[cU_t + \left(\frac{U}{2\lambda} + c_2 U\right)_x\right]_x = \frac{\tau}{2\lambda}U_{xx} = \nu U_{xx} + O(\tau^2), \tag{10}$$

and for the Burgers equation,

$$U_t + \left(\frac{U^2}{2}\right)_x = \tau\left[\left(\frac{U^2}{2}\right)_t + \left(\frac{U}{2\lambda} + \frac{U^3}{4}\right)_x\right]_x = \nu U_{xx} - \left(\frac{\tau}{4}U^2 U_x\right)_x$$

or

$$U_t + \left(\frac{U^2}{2} + \frac{\tau}{4}U^2 U_x\right)_x = \nu U_{xx} + O(\tau^2), \tag{11}$$

where the viscosity v is equal to the ratio of the collision time τ and the equivalent temperature λ. As $v \to 0$, equation (10) reduces to a linear advection equation. However, equation (11) does not reduce to the Burgers equation. In this respect the Burgers equation is not proper to examine the behaviour of the BGK model. However, equation (11) can still be analysed, at least numerically, by subtracting the additional flux $(\tau/4)U^2U_x$ from the BGK flux. Under this modification both equations (10) and (11) become the vanishing viscosity form of the original advection equations when $v \to 0$. This formulation effectively circumvents the problem of differentiability near a discontinuity.[27] Moreover, the vanishing viscosity form is mathematically equivalent to the weak formulation of the advection equations augmented with the entropy condition. Therefore it guarantees a physically correct solution without an entropy fix. From equations (6), (10) and (11) it is concluded that the BGK model properly describes the essential flow physics in both smooth and dissipative regions.

2.2. The gas-kinetic BGK scheme

By integrating the scalar hyperbolic conservation law

$$\frac{\partial U}{\partial t} + \frac{\partial h}{\partial x} = 0$$

over a region $[t_j, t_j + T] \times [x_j - \frac{1}{2}\Delta x, x_j + \frac{1}{2}\Delta x]$, one obtains

$$U_j^{n+1} = U_j^n + \frac{1}{\Delta x}\int_{t^n}^{t^n+T} [h(x_{j-1/2}, t) - h(x_{j+1/2}, t)]\mathrm{d}t,$$

where $U_j^n = (1/\Delta x)\int_{x_j-\Delta x/2}^{x_j+\Delta x/2} U(x, t_n)\mathrm{d}x$ and $\Delta x = x_{j+1} - x_j$. In finite volume gas-kinetic schemes, local solutions of the gas-kinetic equations are used to determine the cell interface flux $h(x_{j+1/2}, t)$. From gas-kinetic theory the numerical flux is given by the first moment of the distribution function:

$$h(x, t) = \int_{-\infty}^{\infty} uf(x, t, u)\mathrm{d}u. \tag{12}$$

The integral solution of the BGK equation (3) for f at the cell boundary $x = x_{j+1/2}$ is[28]

$$f(x_{j+1/2}, t, u) = \frac{1}{\tau}\int_0^t g(x', t', u)\mathrm{e}^{-(t-t')/\tau}\mathrm{d}t' + \mathrm{e}^{-t/\tau}f_0(x_{j+1/2} - ut) \tag{13}$$

for a local constant τ. Here $x' = x_{j+1/2} - u(t - t')$ is a particle trajectory towards $(x_{j+1/2}, t)$ and f_0 is an initial distribution function at $t = 0$. From equations (12) and (13) one may notice that f_0 and g at a cell boundary must be estimated in order to compute a numerical flux.

The initial gas distribution function f_0 usually deviates from a Maxwellian. This is especially noticeable in a discontinuous region. To reflect this fact in the numerical scheme, f_0 is approximated from the interpolated left and right states. In constructing f_0 and g, the first-order slope of space and time variables is considered in this paper. Higher-order slopes could be incorporated in the same manner. Without loss of generality one may assume $x_{j+1/2} = 0$. Then

$$f_0(x, 0, u) = \begin{cases} g_\mathrm{l}(1 + a_\mathrm{l}x/\Delta x) & \text{if } x < 0, \\ g_\mathrm{r}(1 + a_\mathrm{r}x/\Delta x) & \text{if } x > 0, \end{cases} \tag{14}$$

where $g_\mathrm{l} = \sqrt{(\lambda/\pi)}U_\mathrm{l}\mathrm{e}^{-\lambda[u-b(U_\mathrm{l})]^2}$ and $g_\mathrm{r} = \sqrt{(\lambda/\pi)}U_\mathrm{r}\mathrm{e}^{-\lambda[u-b(U_\mathrm{r})]^2}$ are two different Maxwellians and a_l and a_r are related to local slopes. Note that from the results of equation (6), $b(U_\mathrm{l}) = b(U_\mathrm{r}) = c$ for a linear advection equation and $b(U_\mathrm{l}) = U_\mathrm{l}/2$ and $b(U_\mathrm{r}) = U_\mathrm{r}/2$ for the Burgers equation. U_l, U_r, a_l and a_r can be determined from neighbouring data by a proper interpolation principle. Recently Jameson has proposed several numerical schemes based on the LED (local extremum diminishing) principle

that local maxima should not increase and local minima should not decrease.[10,11] Applying the LED principle to U_l, U_r, a_l and a_r, we get

$$U_l = U_j + \tfrac{1}{2}L(\Delta U_{j+1/2}, \Delta U_{j-1/2}), \qquad U_r = U_{j+1} - \tfrac{1}{2}L(\Delta U_{j+1/2}, \Delta U_{j+3/2}),$$

$$a_l = \frac{1}{U_l}L(\Delta U_{j+1/2}, \Delta U_{j-1/2}), \qquad a_r = \frac{1}{U_r}L(\Delta U_{j+1/2}, \Delta U_{j+3/2}),$$

where $\Delta U_{j+1/2} = U_{j+1} - U_j$. $L(u, v)$ is a limiter which will be described in Section 3. Another distribution function g represents an equilibrium state which f approaches. Usually g can be constructed by the Taylor expansion at $x = 0, t = 0$:

$$g = g_0\left(1 + \bar{a}\frac{x}{\Delta x} + At\right), \tag{15}$$

where $g_0 = \sqrt{(\lambda/\pi)}\bar{U}e^{-\lambda[u-b(\bar{U})]^2}$ is a Maxwellian at a cell boundary and $\bar{a}$ is related to the local slope. The velocity $\bar{U}$ in g_0 is the average macroscopic velocity at a cell boundary and A represents the time evolution of g_0. Also, $b(\bar{U}) = c$ for a linear advection equation and $b(\bar{U}) = \bar{U}/2$ for the Burgers equation are used. By applying the compatibility condition at $x = 0, t = 0, g_0$ can be obtained:

$$\int_{-\infty}^{\infty} g_0 \mathrm{d}u = \int_{-\infty}^{\infty} f_0 \mathrm{d}u = \langle u^0, g_l\rangle^+ + \langle u^0, g_r\rangle^-,$$

where $\langle u^n, g\rangle^- \equiv \int_{-\infty}^{0} u^n g \mathrm{d}u$ and $\langle u^n, g\rangle^+ \equiv \int_{0}^{\infty} u^n g \mathrm{d}u$. Thus one obtains

$$\bar{U} = \tfrac{1}{2}[U_l \mathrm{erfc}(-\sqrt{\lambda}b(U_l)) + U_r \mathrm{erfc}(\sqrt{\lambda}b(U_r))],$$

where $\mathrm{erfc}(x)$ is the complementary error function. Note that the upwind biasing average of $\bar{U}$ is naturally obtained at the gas-kinetic level by applying the conservation requirement. The slope $\bar{a}$ in g is an average of the left and right slopes. Simple central differencing should be adequate, since g represents a smooth flow:

$$\bar{a} = \frac{1}{\bar{U}}L(\Delta U_{j-1/2}, \Delta U_{j+3/2}) \quad \text{or} \quad \bar{a} = \frac{1}{\bar{U}}\frac{1}{2}(U_{j+1} - U_j).$$

Owing to its time-evolutionary nature, A cannot be determined from a local interpolation at $t = 0$. The compatibility condition is again applied along the time axis. By substituting equations (14) and (15) into equation (13), the distribution function at time t at a cell boundary is obtained:

$$f(0, t, u) = (1 - e^{-t,\tau})g_0 + [-\tau + (t + \tau)e^{-t/\tau}]u\frac{\bar{a}}{\Delta x}g_0 + (t - \tau + \tau e^{-t/\tau})Ag_0 + e^{-t/\tau}f_0(-ut). \tag{16}$$

By using equations (15) and (16), one has

$$(f - g)(0, t, u) = -e^{-t/\tau}g_0 + [-\tau + (t + \tau)e^{-t/\tau}]u\frac{\bar{a}}{\Delta x}g_0 + \tau(-1 + e^{-t/\tau})Ag_0 + e^{-t/\tau}f_0(-ut).$$

Now the compatibility condition is applied over the CFL time step T,

$$\int_0^T \int_{-\infty}^{\infty} (f - g)\mathrm{d}u\mathrm{d}t = 0, \tag{17}$$

which determines the time evolution term explicitly:

$$A = \beta_1 b(\bar{U})\frac{\bar{a}}{\Delta x} + \frac{1}{2}\beta_2\left[\frac{U_l a_l}{\bar{U}}\left(\mathrm{erfc}(-\sqrt{\lambda}b(U_l))b(U_l) + \frac{\mathrm{e}^{-\lambda b(U_l)^2}}{\sqrt{(\pi\lambda)}}\right)\right.$$
$$\left. + \frac{U_r a_r}{\bar{U}}\left(\mathrm{erfc}(\sqrt{\lambda}b(U_r))b(U_r) - \frac{\mathrm{e}^{-\lambda b(U_r)^2}}{\sqrt{(\pi\lambda)}}\right)\right], \tag{18}$$

where

$$\beta_0 = T - \tau(1 - \mathrm{e}^{-T/\tau}), \qquad \beta_1 = [-T + 2\tau - (2\tau + T)\mathrm{e}^{-T/\tau}]/\beta_0, \qquad \beta_2 = [-\tau + (\tau + T)\mathrm{e}^{-T/\tau}]/\beta_0.$$

Finally, the time-dependent numerical flux at a cell boundary is obtained by taking the first moment of $f(0, t, u)$ with respect to u:

$$\begin{aligned}
h(x_{j+1/2}, t) &= \int_{-\infty}^{\infty} uf(0, t, u)\mathrm{d}u \\
&= \alpha_1\langle u, g_0\rangle + a_2\frac{\bar{a}}{\Delta x}\langle u^2, g_0\rangle + a_3 A\langle u, g_0\rangle + \alpha_4\langle u, f_0\rangle \\
&= \alpha_1\langle u, g_0\rangle + \alpha_2\frac{\bar{a}}{\Delta x}\langle u^2, g_0\rangle + \alpha_3 A\langle u, g_0\rangle + \alpha_4(\langle u, g_l\rangle^+ + \langle u, g_r\rangle^-) \\
&\quad + \alpha_5(a_l\langle u^2, g_l\rangle^+ + a_r\langle u^2, g_r\rangle^-) \\
&= \alpha_1 b(\bar{U})\bar{U} + \frac{\bar{a}}{\Delta x}\alpha_2\left(\frac{\bar{U}}{2\lambda} + b(\bar{U})^2\bar{U}\right) + \alpha_3 A b(\bar{U})\bar{U} \\
&\quad + \alpha_4\left(\frac{b(U_l)}{2}U_l\mathrm{erfc}(-\sqrt{\lambda}b(U_l)) + \frac{\mathrm{e}^{-b(U_l)^2\lambda}}{2\sqrt{(\pi\lambda)}}U_l\right) \\
&\quad + \alpha_4\left(\frac{b(U_r)}{2}U_r\mathrm{erfc}(\sqrt{\lambda}b(U_r)) - \frac{\mathrm{e}^{-b(U_r)^2\lambda}}{2\sqrt{(\pi\lambda)}}U_r\right) \\
&\quad + \alpha_5\left[\frac{1}{2}\left(b(U_l)^2 + \frac{1}{2\lambda}\right)a_l U_l\mathrm{erfc}(-\sqrt{\lambda}b(U_l)) + \frac{b(U_l)\mathrm{e}^{-\lambda b(U_l)^2}}{2\sqrt{(\pi\lambda)}}a_l U_l\right] \\
&\quad + \alpha_5\left[\frac{1}{2}\left(b(U_r)^2 + \frac{1}{2\lambda}\right)a_r U_r\mathrm{erfc}(\sqrt{\lambda}b(U_r)) - \frac{b(U_r)\mathrm{e}^{-\lambda b(U_r)^2}}{2\sqrt{(\pi\lambda)}}a_r U_r\right],
\end{aligned} \tag{19}$$

where

$$\alpha_1 = (1 - \mathrm{e}^{-t/\tau}), \qquad \alpha_2 = [-\tau + (t + \tau)\mathrm{e}^{-t/\tau}], \qquad \alpha_3 = (t - \tau + \tau\mathrm{e}^{-t/\tau}),$$
$$\alpha_4 = \mathrm{e}^{-t/\tau}, \qquad \alpha_5 = -t\alpha_4.$$

In deriving equation (19), we have used again the recurrence relation of $\langle u^n, g\rangle^{\pm}$ and $\langle u^n, g\rangle$ (see Appendix I). The final time-dependent numerical flux is composed of five terms.

The first part $(\alpha_1\langle u, g_0\rangle + \alpha_2(\bar{a}/\Delta x)\langle u^2, g_0\rangle + \alpha_3 A\langle u, g_0\rangle)$ represent a numerical flux which is dominant in a smooth flow. The second part $(\alpha_4(\langle u, g_l\rangle^+ + \langle u, g_r\rangle^-) + \alpha_5(a_l\langle u^2, g_l\rangle^+ + a_r\langle u^2, g_r\rangle^-))$ represents a numerical flux which is dominant in a discontinuous flow. These two parts are coupled in a highly non-linear way based on the BGK gas evolution process. Though the final flux function looks complicated, the analysis in the next section shows the algorithmic structure of the BGK scheme.

2.3. Analysis of the BGK scheme

To analyse the BGK scheme, the numerical flux is rearranged as

$$\begin{aligned} h(x_{j+1/2}, t) &= h_1(x_{j+1,2}, t) + h_2(x_{j+1/2}, t) \\ &= \left(\alpha_1\langle u, g_0\rangle + \alpha_2\frac{\bar{a}}{\Delta x}\langle u^2, g_0\rangle + \alpha_3 A\langle u, g_0\rangle\right) \\ &\quad + \alpha_4[(\langle u, g_l\rangle^+ - ta_l\langle u^2, g_l\rangle^+(\langle u, g_r\rangle^- - ta_r\langle u^2, g^r\rangle^-)]. \end{aligned}$$

Now $h_1(x_{j+1/2}, t)$ can be rewritten as

$$\begin{aligned} h_1(x_{j+1/2}, t) &= \alpha_1\langle u, g_0\rangle + \alpha_2\frac{\bar{a}}{\Delta x}\langle u^2, g_0\rangle + \alpha_3 A\langle u, g_0\rangle \\ &= \left(\langle u, g_0\rangle - \tau\frac{\bar{a}}{\Delta x}\langle u^2, g_0\rangle + (t-\tau)A\langle u, g_0\rangle\right) \\ &\quad - \mathrm{e}^{-t/\tau}\left(\langle u, g_0\rangle - (t+\tau)\frac{\bar{a}}{\Delta x}\langle u^2, g_0\rangle - \tau A\langle u, g_0\rangle\right) \\ &\equiv LW_1(x_{j+1/2}, t) - \mathrm{e}^{-t/\tau}LW_2(x_{j+1/2}, t). \end{aligned}$$

In a smooth region, from equation (14), $f_0(-ut) = g_0[1 - (\bar{a}/\Delta x)ut]$, since the flow can be assumed in an equilibrium state. Then, from equations (16) and (15),

$$(f-g)(0, t, u) = -\tau\alpha_1\left(u\frac{\bar{a}}{\Delta x} + A\right)g_0. \tag{20}$$

By applying the compatibility condition to equation (20), the time evolution term is simplified to

$$A = -b(\bar{U})\frac{\bar{a}}{\Delta x}.$$

Then for a linear advection equation one obtains

$$\begin{aligned} LW_1(x_{j+1/2}, t) &= \langle u, g_0\rangle - \tau\frac{\bar{a}}{\Delta x}\langle u^2, g_0\rangle + (t-\tau)A\langle u, g_0\rangle \\ &= c\bar{U} - \tau\frac{\bar{a}}{\Delta x}\left(\frac{\bar{U}}{2\lambda} + c^2\bar{U}\right) + (t-\tau)\left(-c\frac{\bar{a}}{\Delta x}\right)c\bar{U} \\ &= c\bar{U} - \frac{\bar{a}}{\Delta x}\left(\frac{\tau}{2\lambda}\right)\bar{U} - t\frac{\bar{a}}{\Delta x}c^2\bar{U}, \end{aligned} \tag{21}$$

$$\begin{aligned} LW_2(x_{j+1/2}, t) &= \langle u, g_0\rangle - (\tau+t)\frac{\bar{a}}{\Delta x}\langle u^2, g_0\rangle - \tau A\langle u, g_0\rangle \\ &= c\bar{U} - (\tau+t)\frac{\bar{a}}{\Delta x}\left(\frac{\bar{U}}{2\lambda} + c^2\bar{U}\right) - \tau\left(-c\frac{\bar{a}}{\Delta x}\right)c\bar{U} \\ &= c\bar{U} - \frac{\bar{a}}{\Delta x}\left(\frac{\tau+t}{2\lambda}\right)\bar{U} - t\frac{\bar{a}}{\Delta x}c^2\bar{U}. \end{aligned} \tag{22}$$

From equations (21) and (22) one may notice that LW_1 and LW_2 are in the same form as the numerical flux of the Lax–Wendroff scheme for viscous flow; that is, the numerical flux in an equilibrium state actually represents the Lax-Wendroff scheme at the gas-kinetic level. Thus h_1 can be expressed as

$$h_1(x_{j+1/2}, t) = (1 - \mathrm{e}^{-t/\tau})L\tilde{W}(x_{j+1/2}, t), \qquad L\tilde{W}(x_{j+1/2}, t) = c\bar{U} - \frac{\bar{a}}{\Delta x}\left(\frac{\tilde{\tau}}{2\lambda}\right)\bar{U} - \frac{t\bar{a}}{\Delta x}c^2\bar{U},$$

where $L\tilde{W}(x_{j+1/2)}, t)$ stands for a gas-kinetic Lax–Wendroff flux. Here $\tilde{\tau}$ is τ for equation (21) and $\tau + t$ for equation (22). For the Burgers equation the same analysis leads to

$$L\tilde{W}(x_{j+1/2}, t) = \frac{\bar{U}^2}{2} - \frac{\bar{a}}{\Delta x}\left(\frac{\tilde{\tau}}{2\lambda}\right)\bar{U} - t\frac{\bar{a}}{\Delta x}\frac{\bar{U}^3}{4}.$$

Since this is the flux function for equation (11), it should be modified by $(\tau/4)U^2U_x$. From the compatibility condition,

$$U = \int_{-\infty}^{\infty} g\mathrm{d}u = \int_{-\infty}^{\infty} g_0(1 + At)\mathrm{d}u = \bar{U}(1 + At).$$

Neglecting higher-order time-dependent terms,

$$\frac{\tau}{4}U^2U_x = \frac{\tau}{4}\left(\frac{\bar{a}}{\Delta x}\right)\bar{U}^3(1 + At)^2 \approx \frac{\tau}{4}\left(\frac{\bar{a}}{\Delta x}\right)\bar{U}^3,$$

so

$$L\tilde{W}(x_{j+1/2}, t) = \frac{\bar{U}^2}{2} - \frac{\bar{a}}{\Delta x}\left(\frac{\tilde{\tau}}{2\lambda}\right)\bar{U} - (t + \tau)\frac{\bar{a}}{\Delta x}\frac{\bar{U}^3}{4}. \tag{23}$$

Equation (23) has the same form as the Lax–Wendroff flux. Therefore it can be considered as a gas-kinetic variant of the Lax–Wendroff scheme.

A similar analysis can be done for h_2, which can be written as

$$\begin{aligned} h_2(x_{j+1/2}, t) &= \mathrm{e}^{-t/\tau}[(\langle u, g_\mathrm{l}\rangle^+ - ta_\mathrm{l}\langle u^2, g_\mathrm{l}\rangle^+) + (\langle u, g_\mathrm{r}\rangle^- - ta_\mathrm{r}\langle u^2, g_\mathrm{r}\rangle^-)] \\ &= \mathrm{e}^{-t/\tau}(KF^+ + KF^-), \end{aligned}$$

where

$$KF^+(x_{j+1/2}, t) = \langle u, g_\mathrm{l}\rangle^+ - ta_\mathrm{l}\langle u^2, g_\mathrm{l}\rangle^+, \tag{24}$$

$$KF^-(x_{j+1/2}, t) = \langle u, g_\mathrm{r}\rangle^- - ta_\mathrm{r}\langle u^2, g_\mathrm{r}\rangle^-. \tag{25}$$

For the sake of convenience, only a first-order flux with $a_\mathrm{l} = a_\mathrm{r} = 0$ is considered. Then for a linear advection equation one obtains

$$\begin{aligned} KF^+(x_{j+1/2}, t) &= \langle u, g_\mathrm{l}\rangle^+ \\ &= \frac{c}{2}U_\mathrm{l}\mathrm{erfc}(-\sqrt{c}) + \frac{\mathrm{e}^{-\lambda c^2}}{2\sqrt{(\pi\lambda)}}U_\mathrm{l} \\ &= \frac{c}{2}U_\mathrm{l}[1 + \mathrm{erf}(\sqrt{\lambda}c)] + \frac{\mathrm{e}^{-\lambda c^2}}{2\sqrt{(\pi\lambda)}}U_\mathrm{l}, \end{aligned} \tag{26}$$

$$\begin{aligned} KF^-(x_{j+1/2}, t) &= \langle u, g_\mathrm{r}\rangle^- \\ &= \frac{c}{2}U_\mathrm{r}[1 - \mathrm{erf}(\sqrt{\lambda}c)] - \frac{\mathrm{e}^{-\lambda c^2}}{2\sqrt{(\pi\lambda)}}U_\mathrm{r}. \end{aligned} \tag{27}$$

Similarly for the Burgers equation one may obtain

$$KF^+(x_{j+1/2}, t) = \langle u, g_l \rangle^+ = \frac{U_l^2}{4}\left[1 + \operatorname{erf}\left(\sqrt{\lambda}\frac{U_l}{2}\right)\right] + \frac{e^{-\lambda U_l^2/4}}{2\sqrt{(\pi\lambda)}}U_l, \tag{28}$$

$$KF^-(x_{j+1/2}, t) = \langle u, g_r \rangle^- = \frac{U_r^2}{4}\left[1 - \operatorname{erf}\left(\sqrt{\lambda}\frac{U_r}{2}\right)\right] - \frac{e^{-\lambda U_r^2/4}}{2\sqrt{(\pi\lambda)}}U_r. \tag{29}$$

Equations (26) and (27) and equations (28) and (29) are identical with kinetic flux vector splitting based on the collisionless Boltzmann equation.[22] By the same procedure one may show that equations (24) and (25) are the same as the numerical flux of second-order kinetic flux vector splitting. Therefore h_2 is expressed as

$$h_2(x_{j+1/2}, t) = e^{-t/\tau}[KF^+(x_{j+1/2}, t) + KF^-(x_{j+1/2}, t)].$$

Finally, the numerical flux of the BGK scheme can be expressed as

$$h(x_{j+1/2}, t) = h_1(x_{j+1/2}, t) + h_2(x_{j+1/2}, t) = (1 - e^{-t/\tau})L\tilde{W}(x_{j+1/2}, t) + e^{-t/\tau}(KF^+ + KF^-) \tag{30}$$

or

$$h(x_{j+1/2}, t) = L\tilde{W}(x_{j+1/2}, t) + e^{-t/\tau}[(KF^+ + KF^-) - L\tilde{W}(x_{j+1/2}, t)]. \tag{31}$$

Thus the BGK scheme combines the GKLW (gas-kinetic Lax–Wendroff) scheme with KFVS (kinetic flux vector splitting) and these two basic schemes are correlated through collision time or, equivalently, viscosity. Some conclusions can be drawn from equations (30) and (31).

First, the two basic parts in the BGK scheme offer an intrinsic multidimensional extension. It is known that a multidimensional form of the Lax–Wendroff scheme can be obtained for systems of equations, although the estimation of the Jacobian matrix is expensive. In the GKLW scheme, multidimensionality can be achieved by the interpolation of the equilibrium distribution function g. On the other hand, multidimensional KFVS can be achieved by the interpolation of the initial non-equilibrium distribution function f_0 without resorting to wave modelling.[22] The multidimensionality of the BGK scheme can also be seen from the form of a distribution function. In a three-dimensional advection equation the particle distribution function can be expressed as

$$g = Ae^{-\lambda[(u-U)^2+(v-V)^2+(w-W)^2]},$$

where (u, v, w) are particle velocities and (U, V, W) are macroscopic velocities. Then the shape of the distribution function is determined by the contribution of all macroscopic velocities and random motions of particle velocities in phase space, not by the superposition of each velocity component. Thus the flux derived from the moments of the distribution function naturally considers the multidimensionality. At this stage an initial interpolation technique which reflects the multi-dimensionality should be introduced.

Second, from equation (31) one may find that the BGK scheme fully utilizes the flow physics in a smooth region. Based on the BGK flux, the GKLW flux is modified by the gas-kinetic limiter ($e^{-t/r}$) which captures the imbalance between GKLW and KFVS. This may be clearly seen if one considers the first-order flux of the BGK scheme, where GKLW reduces to a central differencing type of flux, although g_0 is constructured according to the upwind biasing property in the gas-kinetic level.

Third, since the BGK scheme is identified as a combination of GKLW and KFVS, one may derive a simplified BGK scheme which maintains the essential properties of the original BGK scheme. One promising variant is

$$f(0, t, u) = (1 - e^{-t/\tau})g_0\left(1 - \frac{\bar{a}}{\Delta x}u(t + \tau) + At\right) + e^{-t/\tau}f_0(-ut), \tag{32}$$

where the time evolution term A can be approximated as $-b(\bar{U})\bar{a}/\Delta x$. One may find that the structure for the numerical flux of equation (32) is the same as equation (30), although there is a difference in evaluating A.

3. NUMERICAL RESULTS

Since the physical thickness of a shock wave is much thinner than the grid size (Δx), artificial dissipation must be introduced to enlarge discontinuities to a scale comparable with the grid size. In the BGK scheme the viscosity is controlled by the collision time. The collision time is defined as

$$\tau = \tau_1 + \tau_2.$$

Here τ_1 is the collision time related to the physical viscosity, which is usually very small compared with the CFL time step, and τ_2 is the artificial dissipation to resolve discontinuities. In the case of systems of equations such as the Euler or Navier–Stokes equations, τ_1 can be determined *analytically* and τ_2 is determined by using a pressure-type switch. In the case of a scalar equation, however, there are not enough conditions to fix τ_1. Therefore τ_1 is fixed to a small value compared with the CFL time step and the following form of the collision time has been employed in all test cases:

$$\tau = 0{\cdot}01 + 0{\cdot}5\ \mathrm{Max}(w_1, w_2),$$

where

$$w_1 = \frac{|U_{j+1} - 2U_j + U_{j-1}|}{|U_{j+1} - U_j| + |U_j - U_{j-1}|}, \qquad w_2 = \frac{|U_{j+2} - 2U_{j+1} + U_j|}{|U_{j+2} - U_{j+1}| + |U_{j+1} - U_j|}.$$

Another parameter to be determined is λ. As mentioned in Section 2, λ controls the dispersion of a distribution function and this is again determined analytically from macroscopic variables for systems of equations. In all numerical test cases λ is fixed at 100. Here we again emphasize that numerical results are not very sensitive to variation in τ_1 or λ and λ is determined *analytically*[24] for systems of equations. We also mention that τ_2 adopted in this paper is not the best choice, because we can get much better results than presented in this paper by changing the coefficient of τ_2 for each test case. However, we have used a fixed τ_2 for all test cases in order to keep the robustness of the numerical schemes.

In the interpolation stage described in Section 2, many limiters can be used in constructing f_0 or g. The following standard limiters are employed to observe their effects and compare corresponding current higher-order shock-capturing schemes:

(1) Minmod

$$L(u, v) = S(u, v)\mathrm{Min}(u, v),$$

(2) van Leer

$$L(u, v) = S(u, v)\frac{2|u||v|}{|u| + |v|},$$

(3) Superbee

$$L(u, v) = S(u, v)\text{Max}(\text{Min}(2|u|, |v|), \text{Min}(|u|, 2|v|)),$$

(4) α-mean with $\alpha = 2$ (MUSCL)

$$L(u, v) = S(u, v)\text{Min}\left(\frac{|u| + |v|}{2}, 2|u|, 2|v|\right),$$

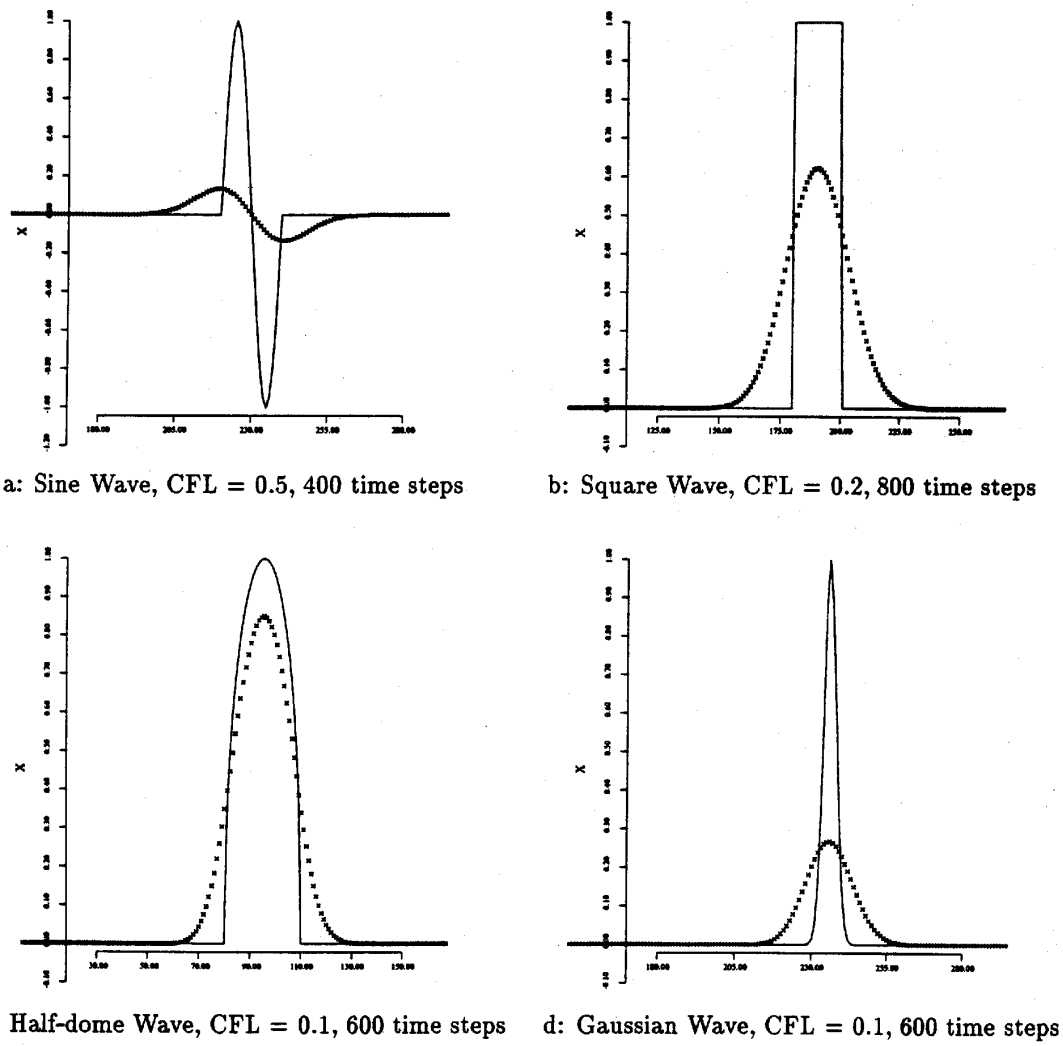

Figure 1. Linear advection with first-order BGK scheme. Computed results (×) are compared with exact solutions (—)

(5) second-order ENO

$$L(u, v) = S(u, v)\mathrm{Min}(u, v),$$

$$u = d_{j-1/2}w + \tfrac{1}{2}D_{j-1/2}w, \qquad v = d_{j+1/2}w - \tfrac{1}{2}D_{j+1/2}w,$$

$$d_{j+1/2}w = w_{j+1} - w_j, \qquad D_{j+1/2}w = \mathrm{Min}(d_{j+1/2}w - d_{j-1/2}w, d_{j+3/2}w - d_{j+1/2}w),$$

where $S(u, v) = \frac{1}{2}[\mathrm{sign}(u) + \mathrm{sign}(v)]$. Six different schemes including a first-order scheme have been tested for advection equations. For gas-dynamic systems, several results of higher-order BGK schemes using the MUSCL limiter are presented.

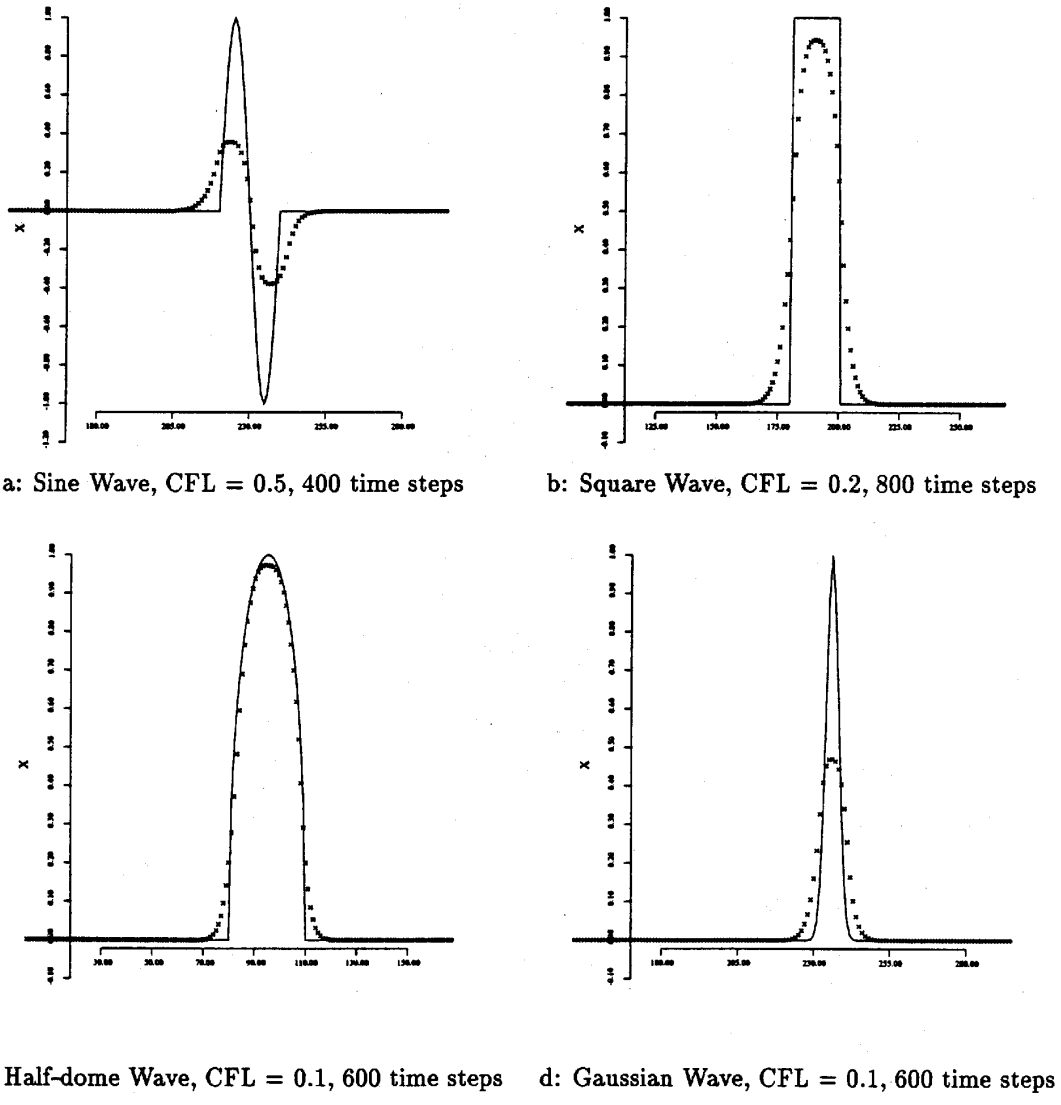

a: Sine Wave, CFL = 0.5, 400 time steps

b: Square Wave, CFL = 0.2, 800 time steps

c: Half-dome Wave, CFL = 0.1, 600 time steps

d: Gaussian Wave, CFL = 0.1, 600 time steps

Figure 2. Linear advection with Minmod-BGK scheme. Computed results (×) are compared with exact solutions (—)

3.1. Advection equations

For a linear advection equation the BGK schemes are tested with four different initial profiles: a sine wave, a square wave, a half-dome wave and a Gaussian wave. The last three initial profiles have been widely used to check the behaviour of various numerical schemes[1,29,30] in both smooth and discontinuous regions. For a sine wave the CFL number is 0·5 with 400 time steps and for the other test cases the CFL numbers and time steps are the same as in Reference 30. Figures 1–6 show the results of each test case. In the case of the first-order BGK scheme the computed results are smeared over many cells owing to the large numerical diffusion, which is expected (Figure 1). However, the higher-order BGK schemes not only capture discontinuities crisply but also produce excellent results in smooth regions, except for the Minmod-BGK scheme (Figures 2–6). The effect of limiters, i.e. the effect of interpolation techniques, is visible. The Superbee-BGK scheme produces very high peaks

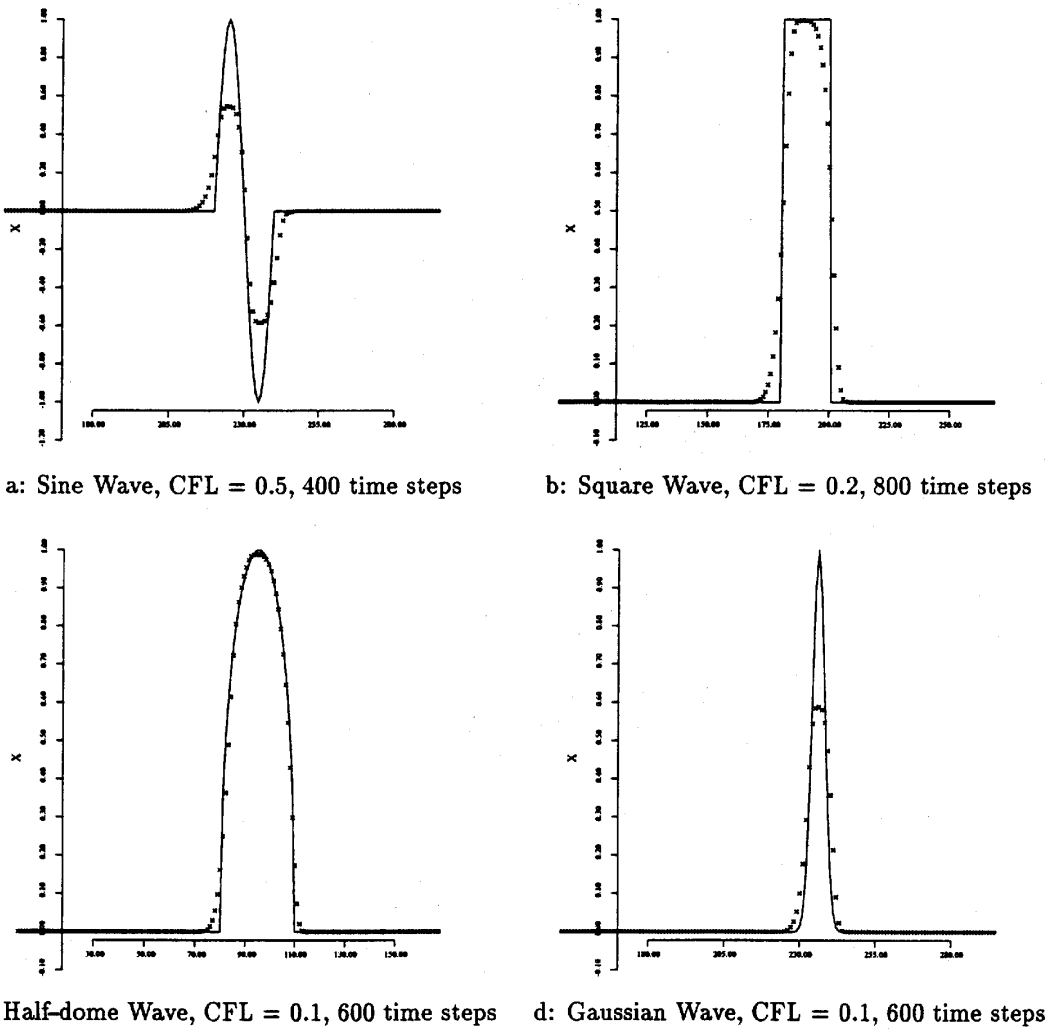

Figure 3. Linear advection with van Leer-BGK scheme. Computed results (×) are compared with exact solutions (—)

and sharp discontinuities but oscillates around the top of a half-dome wave (Figure 5), while the ENO-BGK scheme shows an opposite behaviour (Figure 6) approximately. Judging from the overall performance, the MUSCL-BGK scheme seems go give the best results (Figure 4). Comparing the results of the BGK schemes with those of current advanced shock-capturing schemes,[30] the BGK schemes give competitive results or better accuracy for some test cases such as a half-dome wave or a Gaussian wave.

In the case of the Burgers equation, three different initial profiles—a square wave, a sine wave and a staircase wave—are tested. The formation and propagation of discontinuities are compared with analytical solutions at two different times for each test case. Similar to the case of a linear advection equation, the first-order BGK scheme is rather diffusive but captures discontinuities within two or three interior points (Figures 7–9). All the other schemes except for the Minmod-BGK scheme give excellent results in capturing discontinuities or in smooth regions including sharp corners (Figures

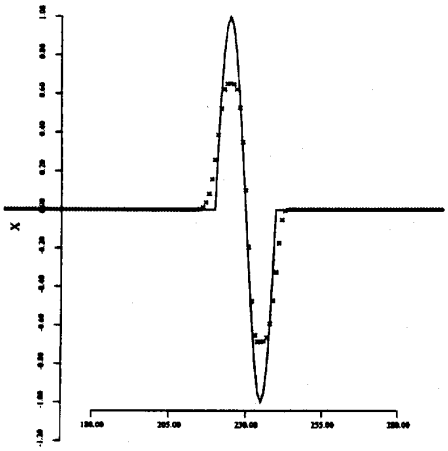

a: Sine Wave, CFL = 0.5, 400 time steps

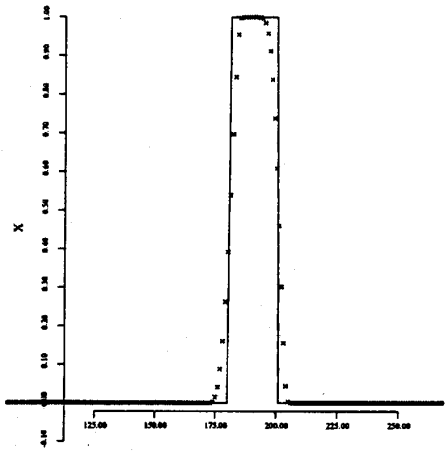

b: Square Wave, CFL = 0.2, 800 time steps

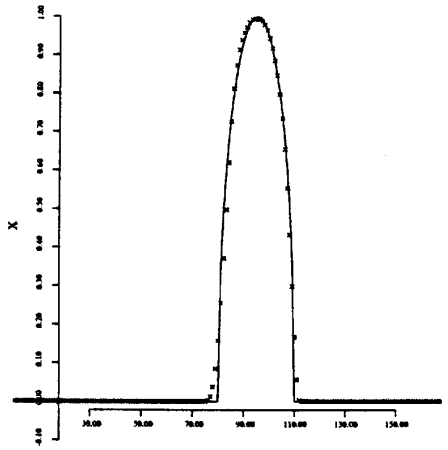

c: Half-dome Wave, CFL = 0.1, 600 time steps

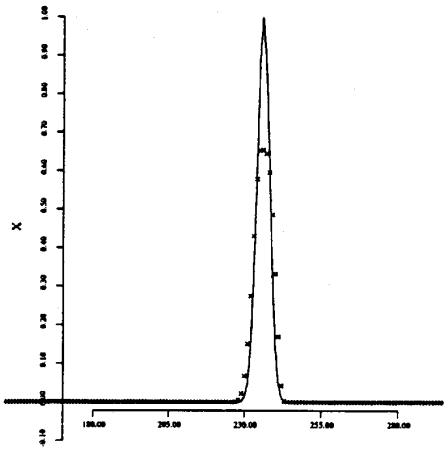

d: Gaussian Wave, CFL = 0.1, 600 time steps

Figure 4. Linear advection with MUSCL-BGK scheme. Computed results (×) are compared with exact solutions (—)

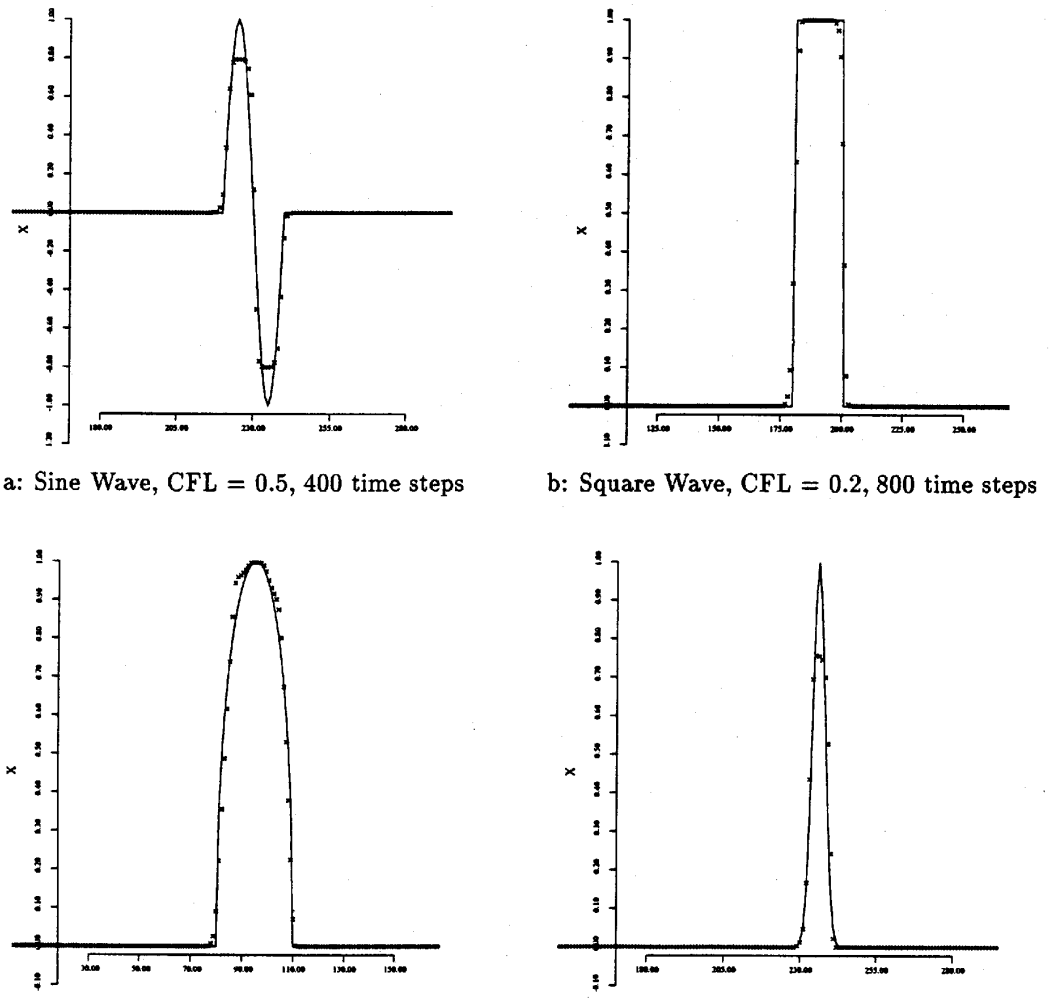

a: Sine Wave, CFL = 0.5, 400 time steps

b: Square Wave, CFL = 0.2, 800 time steps

c: Half-dome Wave, CFL = 0.1, 600 time steps

d: Gaussian Wave, CFL = 0.1, 600 time steps

Figure 5. Linear advection with Superbee-BGK scheme. Computed results (×) are compared with exact solutions (—)

10–24). Judging from the comparison,[31,32] one may confirm again the higher-resolution property of the BGK scheme that has been analysed in Section 2.

As we can see from equation (32), efficient versions of the original BGK scheme can be derived by simplifying the construction of f_0 and g in the gas evolution stage.

3.2. Application to gas-dynamic equations

The BGK flux for the Euler or Navier–Stokes equations can be constructed in a similar manner as described in Section 2 without major changes.[24,25] The evolution of gas-dynamic systems, however, is much more complex than that of simple advection equations, mainly owing to linear and non-linear wave interactions. This poses additional issues such as the positivity condition, interpolation techniques, construction of interface states, etc. These problems should be reflected properly in

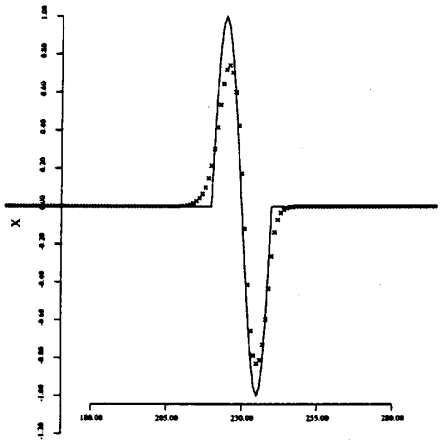

a: Sine Wave, CFL = 0.5, 400 time steps

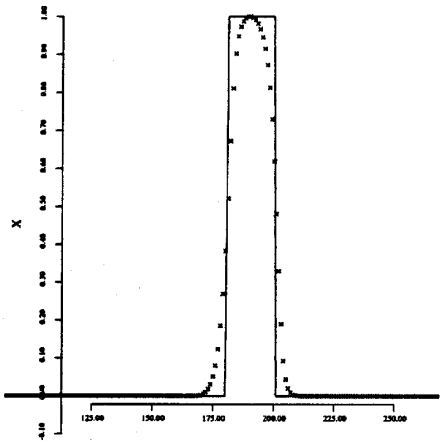

b: Square Wave, CFL = 0.2, 800 time steps

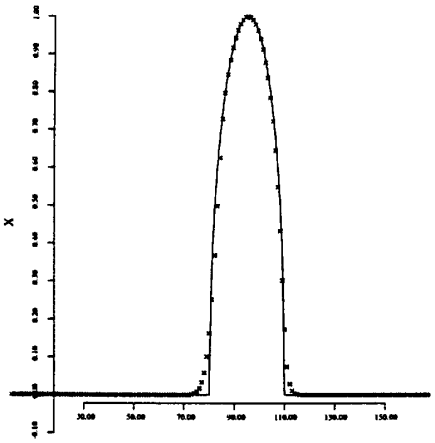

c: Half-dome Wave, CFL = 0.1, 600 time steps

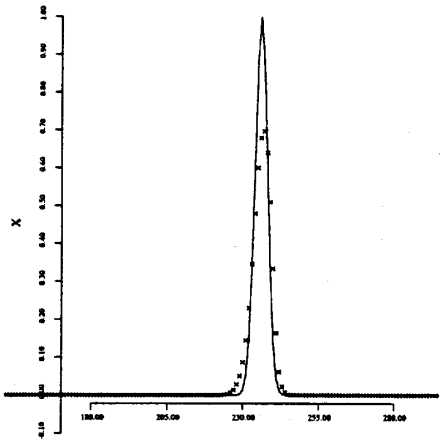

d: Gaussian Wave, CFL = 0.1, 600 time steps

Figure 6. Linear advection with ENO-BGK scheme. Computed results (×) are compared with exact solutions (—)

formulating fluxes to get an accurate and robust scheme. Recent work has shown that BGK schemes possess desirable properties for such problems. In the present work we will omit this part and simply present several results for well-known test cases. A complete description of the BGK solver for gas-dynamic systems is given in Reference 26. Figures 25 and 26 show the results of standard shock tube and blast wave problems. The cell distribution and CFL time step are the same as in References 7 and 9. Comparing the results with those of References 7 and 9, one observes that the BGK solver gives results better than FCT or second-order ENO and competitive with MUSCL, fourth-order ENO or PPM for the resolution of shock waves or contact discontinuities as well as smooth flow regions. Figure 27 shows two-dimensional examples of the unsteady Euler equations. In the shock ramp calculations (Figure 27b) the wall jet is relatively diffuse in comparison with the PPM scheme. This is probably due to the fact that the current BGK scheme uses a second-order initial interpolation (MUSCL limiter) without any artificial sharpening technique and the solver itself yields a Navier–

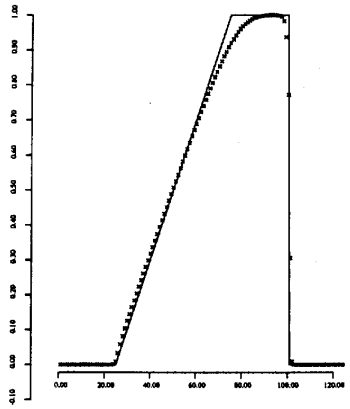

a: Square Wave, CFL = 0.5, 100 time steps

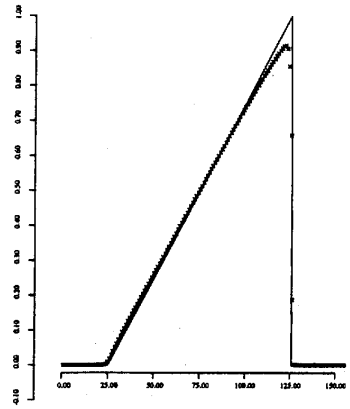

b: Square Wave, CFL = 0.5, 200 time steps

Figure 7. Burgers equation with first-order BGK scheme. Computed results (×) are compared with exact solutions (—)

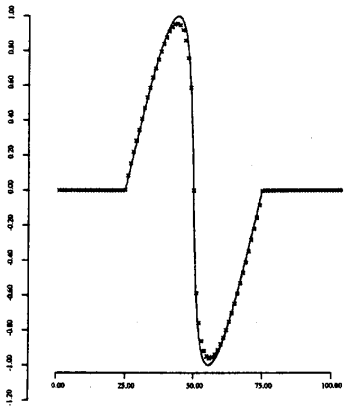

a: Sine Wave, CFL = 0.2, 35 time steps

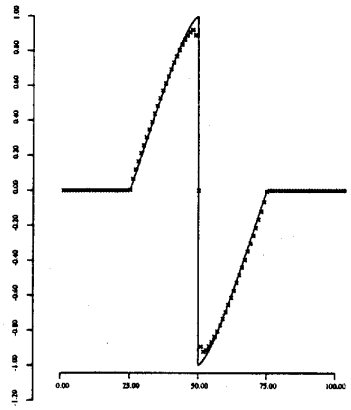

b: Sine Wave, CFL = 0.2, 65 time steps

Figure 8. Burgers equation with first-order BGK scheme. Computed results (×) are compared with exact solutions (—)

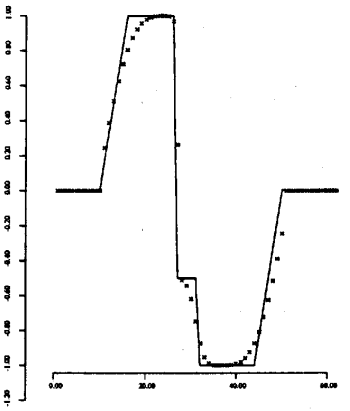

a: Stair Wave, CFL = 0.5, 12 time steps

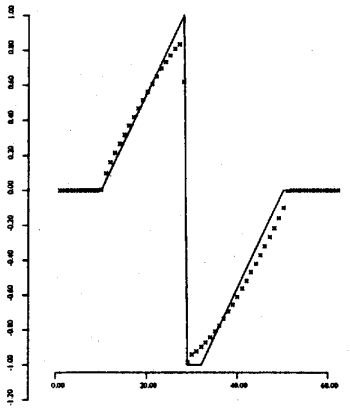

b: Stair Wave, CFL = 0.5, 36 time steps

Figure 9. Burgers equation with first-order BGK scheme. Computed results (×) are compared with exact solutions (—)

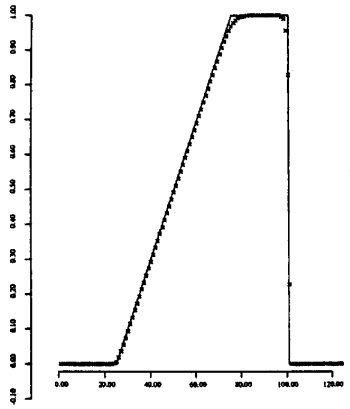

a: Square Wave, CFL = 0.5, 100 time steps

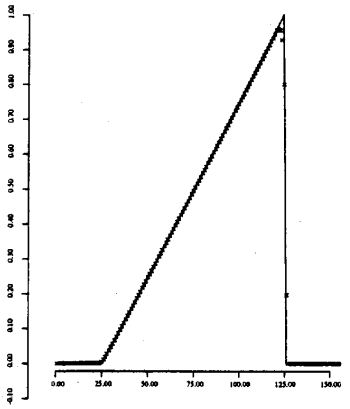

b: Square Wave, CFL = 0.5, 200 time steps

Figure 10. Burgers equation with Minmod-BGK scheme. Computed results (×) are compared with exact solutions (—)

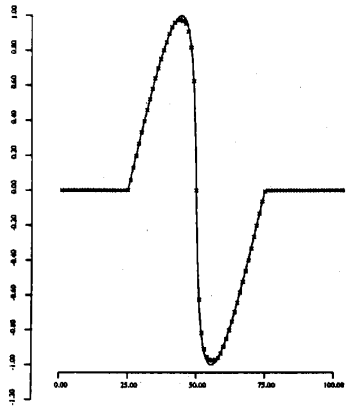

a: Sine Wave, CFL = 0.2, 35 time steps

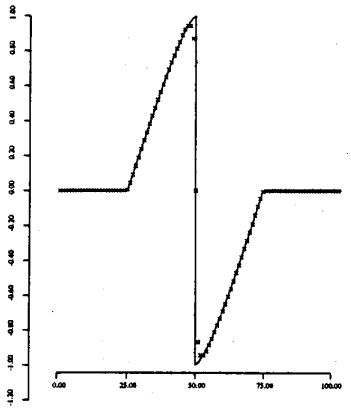

b: Sine Wave, CFL = 0.2, 65 time steps

Figure 11. Burgers equation with Minmod-BGK scheme. Computed results (×) are compared with exact solutions (—)

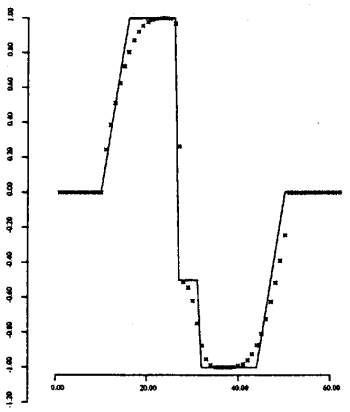

a: Stair Wave, CFL = 0.5, 12 time steps

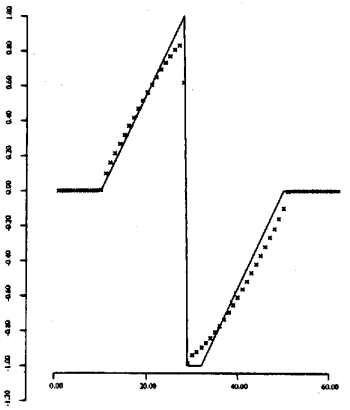

b: Stair Wave, CFL = 0.5, 36 time steps

Figure 12. Burgers equation with Minmod-BGK scheme. Computed results (×) are compared with exact solutions (—)

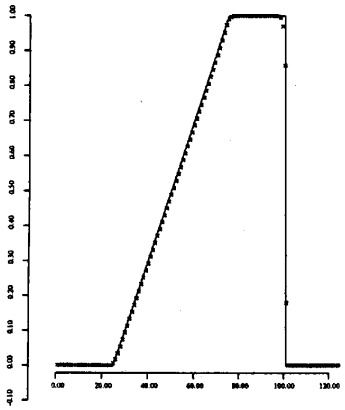

a: Square Wave, CFL = 0.5, 100 time steps

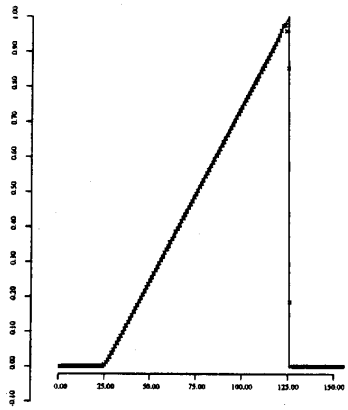

b: Square Wave, CFL = 0.5, 200 time steps

Figure 13. Burgers equation with van Leer-BGK scheme. Computed results (×) are compared with exact solutions (—)

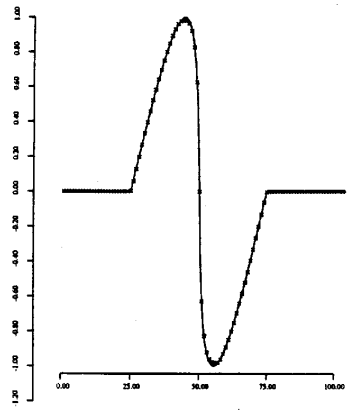

a: Sine Wave, CFL = 0.2, 35 time steps

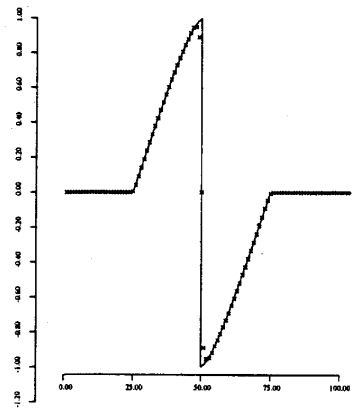

b: Sine Wave, CFL = 0.2, 65 time steps

Figure 14. Burgers equation with van Leer-BGK scheme. Computed results (×) are compared with exact solutions (—)

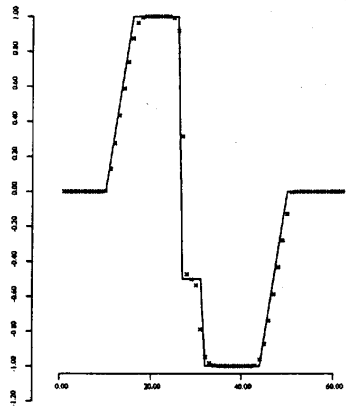

a: Stair Wave, CFL = 0.5, 12 time steps

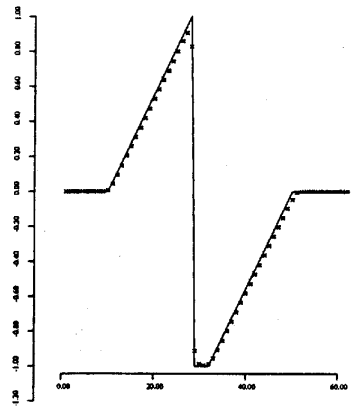

b: Stair Wave, CFL = 0.5, 36 time steps

Figure 15. Burgers equation with van Leer-BGK scheme. Computed results (×) are compared with exact solutions (—)

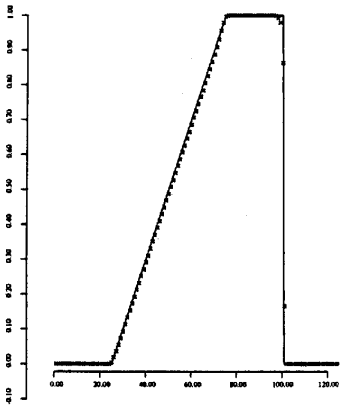

a: Square Wave, CFL = 0.5, 100 time steps

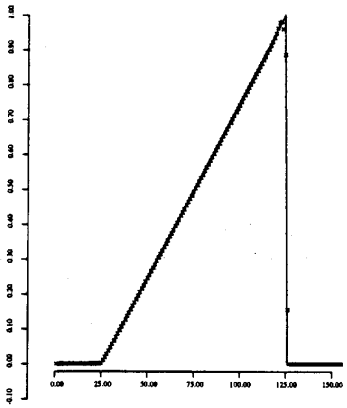

b: Square Wave, CFL = 0.5, 200 time steps

Figure 16. Burgers equation with MUSCL-BGK scheme. Computed results (×) are compared with exact solutions (—)

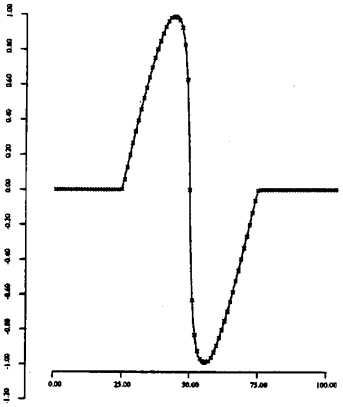

a: Sine Wave, CFL = 0.2, 35 time steps

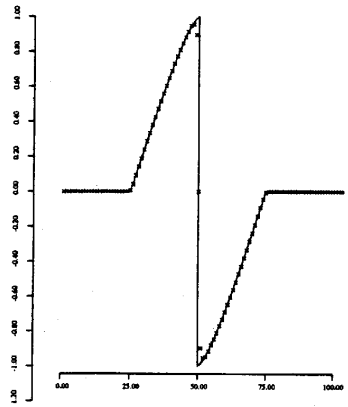

b: Sine Wave, CFL = 0.2, 65 time steps

Figure 17. Burgers equation with MUSCL-BGK scheme. Computed results (×) are compared with exact solutions (—)

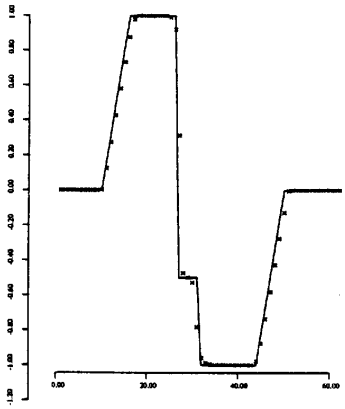

a: Stair Wave, CFL = 0.5, 12 time steps

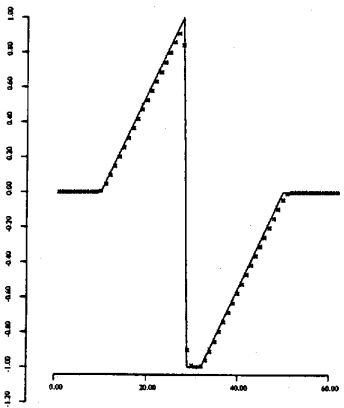

b: Stair Wave, CFL = 0.5, 36 time steps

Figure 18. Burgers equation with MUSCL-BGK scheme. Computed results (×) are compared with exact solutions (—)

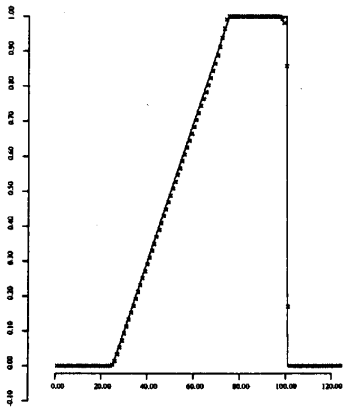

a: Square Wave, CFL = 0.5, 100 time steps

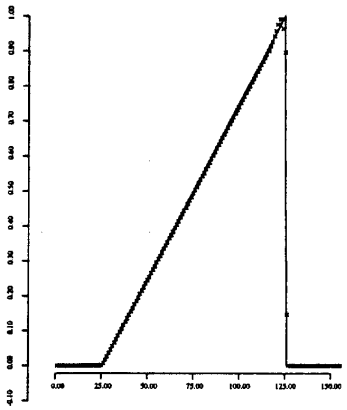

b: Square Wave, CFL = 0.5, 200 time steps

Figure 19. Burgers equation with Superbee-BGK scheme. Computed results (×) are compared with exact solutions (—)

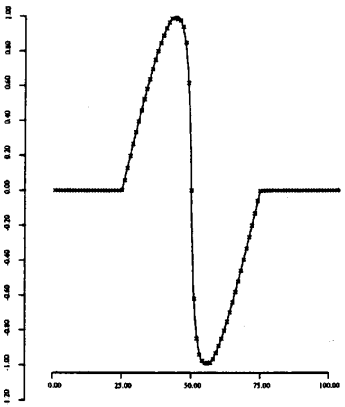

a: Sine Wave, CFL = 0.2, 35 time steps

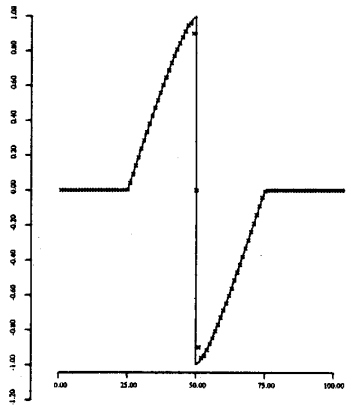

b: Sine Wave, CFL = 0.2, 65 time steps

Figure 20. Burgers equation with Superbee-BGK scheme. Computed results (×) are compared with exact solutions (—)

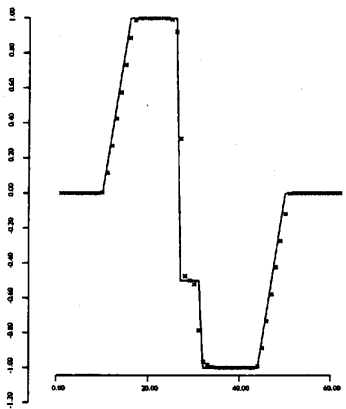

a: Stair Wave, CFL = 0.5, 12 time steps

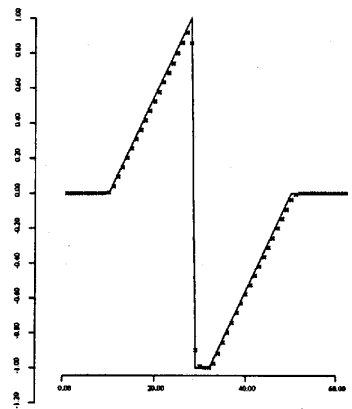

b: Stair Wave, CFL = 0.5, 36 time steps

Figure 21. Burgers equation with Superbee-BGK scheme. Computed results (×) are compared with exact solutions (—)

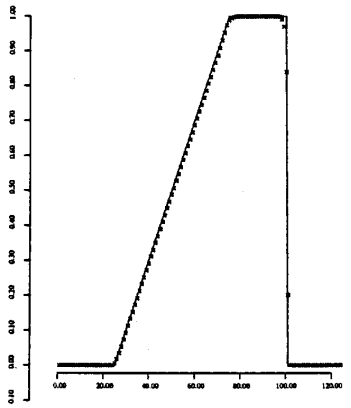

a: Square Wave, CFL = 0.5, 100 time steps

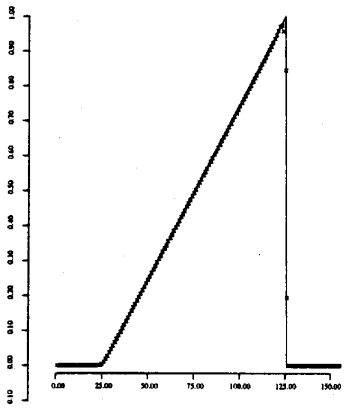

b: Square Wave, CFL = 0.5, 200 time steps

Figure 22. Burgers equation with ENO-BGK scheme. Computed results (×) are compared with exact solutions (—)

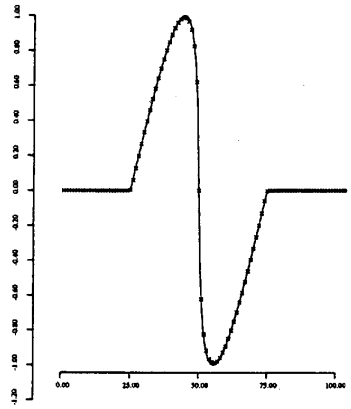

a: Sine Wave, CFL = 0.2, 35 time steps

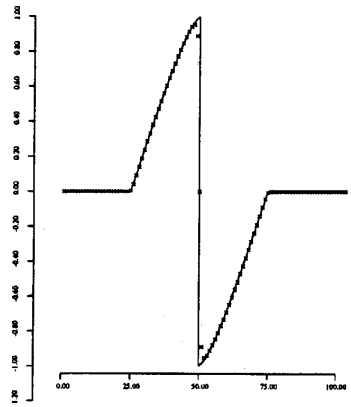

b: Sine Wave, CFL = 0.2, 65 time steps

Figure 23. Burgers equation with ENO-BGK scheme. Computed results (×) are compared with exact solutions (—)

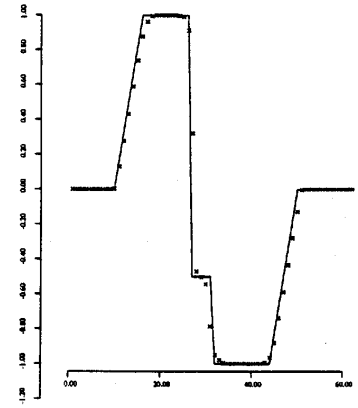

a: Stair Wave, CFL = 0.5, 12 time steps

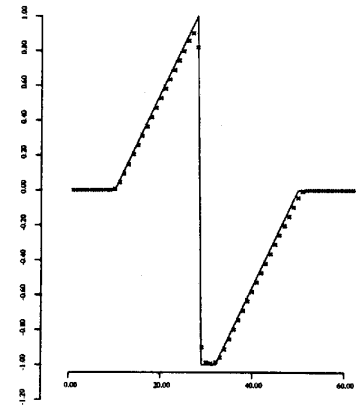

b: Stair Wave, CFL = 0.5, 36 time steps

Figure 24. Burgers equation with ENO-BGK scheme. Computed results (×) are compared with exact solutions (—)

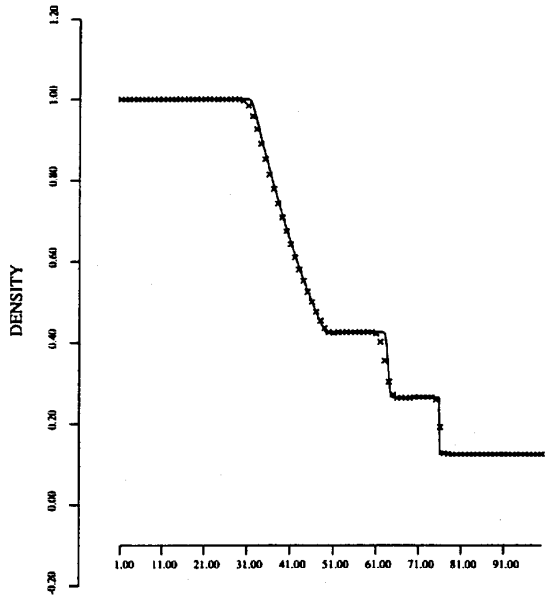

a: Sod test case

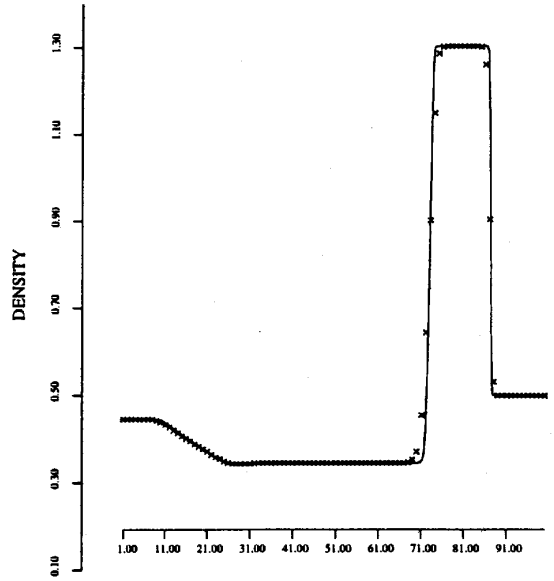

b: Harten-Lax test case

Figure 25. Shock tube problem with MUSCL-BGK scheme. Computed results (×, 100 cells) are compared with exact solutions (—)

Stokes equation. Also, the particle diffusion is an intrinsic property in the gas-kinetic description. It is probabaly important to study in detail the particle diffusion effect in the current BGK scheme in the future. A rigorous comparison of computational efficiency is difficult since it depends on programming skills among other factors. According to our experience, however, the CPU time required by a BGK solver is comparable with that of a second-order Roe scheme with entropy fixes.

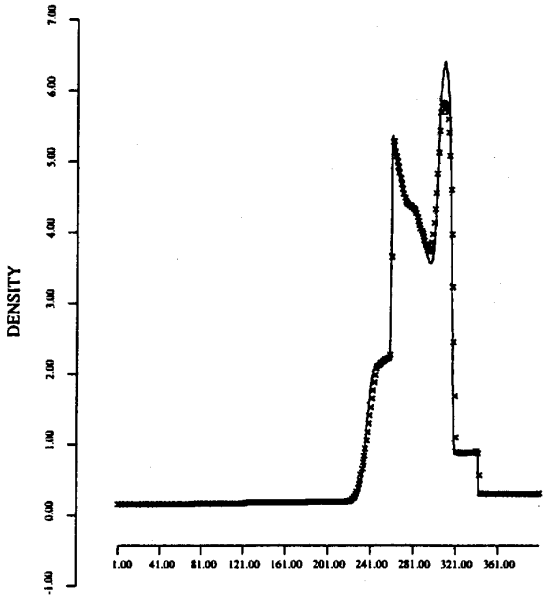

Figure 26. Blast wave problem with MUSCL-BGK scheme. Computed results (× , 400 cells) are compared with 800-cell calculation (—)

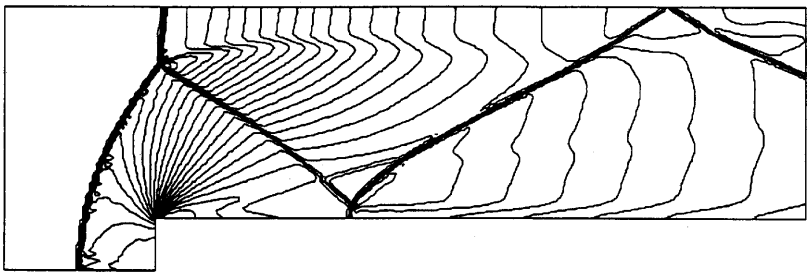

a: Forward Facing Step (M = 3, 240*80 cells)

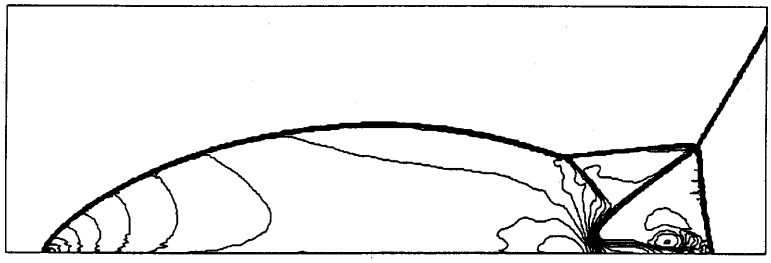

b: Double Mach Reflection (M = 10, 360*120 cells)

Figure 27. Density Distributions with MUSCL-BGK scheme

4. CONCLUSIONS

In the present work the issue of errors caused by a gas evolution model as well as interpolation principles has been addressed. The BGK flux function is analysed by reconstructing advection equations and implemented for both advection equations and gas-dynamic systems. A family of higher-order gas-kinetic BGK schemes is derived using limiters. The resultant schemes are a combination of a gas-kinetic Lax–Wendroff flux and kinetic flux vector splitting, i.e. a combination of central differencing flux and upstream differencing flux. This result contrasts the BGK model with Riemann solver, because the numerical flux of a Riemann solver for advection equations reduces to pure upwinding. The analysis presented in this work shows that the BGK model provides a more physical gas evolution process than a Riemann solver in three important aspects.

Firstly, any higher-order slope of flow variables in the interpolation stage can be readily accounted for in constructing a time-dependent distribution function at a cell boundary. These slopes are included during the CFL time step to obtain the final numerical fluxes. Thus the BGK model can describe a higher-order gas evolution process.

Secondly, the intrinsic random motion of particles is implicitly included in the form of the distribution function. From this fact a multidimensional gas-kinetic scheme can be obtained by introducing multidimensional interpolation of f_0 and g without using macroscopic wave modelling.

Thirdly, since the BGK model essentially describes the gas evolution process of viscous flow, the gas-kinetic scheme based on the BGK model always satisfies the entropy condition.

These three properties can be fully exploited to produce a better numerical scheme.

ACKNOWLEDGEMENTS

The research in the present paper is supported by Grant URI/AFOSR F49620-93-1-0427 for all authors. The first author is also thankful for the financial support provided by the Ministry of Education in Korea. We also thank the referees for constructive comments on an earlier version of this manuscript.

APPENDIX I: RECURRENCE RELATIONS OF MOMENTS OF A DISTRIBUTION FUNCTION

From its construction,

$$\langle u^0, g\rangle = \int_{-\infty}^{\infty} g\mathrm{d}u = A\int_{-\infty}^{\infty} \mathrm{e}^{-\lambda[u-b(U)]^2}\mathrm{d}u = \frac{2A}{\sqrt{\lambda}}\int_0^{\infty} \mathrm{e}^{-t^2}\mathrm{d}t = \frac{2A}{\sqrt{\lambda}}\left(\frac{\sqrt{\pi}}{2}\right) = U.$$

Thus we get $A = \sqrt{(\lambda/\pi)}U$. Also, we get

$$\begin{aligned}\langle u, g\rangle &= \int_{-\infty}^{\infty} gu\mathrm{d}u = U\sqrt{\left(\frac{\lambda}{\pi}\right)}\int_{-\infty}^{\infty} \mathrm{e}^{-\lambda[u-b(U)]^2}u\mathrm{d}u \\ &= U\sqrt{\left(\frac{\lambda}{\pi}\right)}\frac{b(U)}{\sqrt{\lambda}}[\lambda\pi\mathrm{erf}(\infty)] = b(U)U.\end{aligned}$$

Similarly, we may obtain

$$\begin{aligned}\langle u^0, g\rangle^+ &= \int_0^\infty g\mathrm{d}u = U\sqrt{\left(\frac{\lambda}{\pi}\right)}\int_0^\infty \mathrm{e}^{-\lambda[u-b(U)]^2}\mathrm{d}u \\ &= U\sqrt{\left(\frac{\lambda}{\pi}\right)}\left(\frac{\sqrt{\pi}}{2\sqrt{\lambda}}\mathrm{erfc}(-b(U)\sqrt{\lambda})\right) \\ &= \frac{U}{2}\mathrm{erfc}(-b(U)\sqrt{\lambda}),\end{aligned}$$

$$\begin{aligned}\langle u, g\rangle^+ &= \int_0^\infty gu\mathrm{d}u = U\sqrt{\left(\frac{\lambda}{\pi}\right)}\int_0^\infty \mathrm{e}^{-\lambda[u-b(U)]^2}u\mathrm{d}u \\ &= U\sqrt{\left(\frac{\lambda}{\pi}\right)}\left[\frac{1}{\lambda}\int_{-b(U)\sqrt{\lambda}}^\infty \mathrm{e}^{-t^2}\left(\frac{t}{\sqrt{\lambda}}+b(U)\right)\frac{\mathrm{d}t}{\sqrt{\lambda}}\right] \\ &= b(U)\frac{U}{2}\mathrm{erfc}(-b(U)\sqrt{\lambda}) + \frac{U}{2\sqrt{(\pi\lambda)}}\mathrm{e}^{-b(U)^2\lambda},\end{aligned}$$

$$\langle u^0, g\rangle^- = \frac{U}{2}\mathrm{erfc}(b(U)\sqrt{\lambda}), \qquad \langle u, g\rangle^- = b(U)\frac{U}{2}\mathrm{erfc}(b(U)\sqrt{\lambda}) - \frac{U}{2\sqrt{(\pi\lambda)}}\mathrm{e}^{-b(U)^2\lambda}.$$

Now we simply apply integration by parts $\langle u^n, g\rangle$:

$$\begin{aligned}\langle u^n, g\rangle &= \int_{-\infty}^\infty gu^n\mathrm{d}u = U\sqrt{\left(\frac{\lambda}{\pi}\right)}\int_{-\infty}^\infty \mathrm{e}^{-\lambda[u-b(U)]^2}u^n\mathrm{d}u \\ &= U\sqrt{\left(\frac{\lambda}{\pi}\right)}\left(\frac{2\lambda}{n+1}\int_{-\infty}^\infty \mathrm{e}^{-\lambda[u-b(U)]^2}u^{n+2}\mathrm{d}u - \frac{2\lambda b(U)}{n+1}\int_{-\infty}^\infty \mathrm{e}^{-\lambda[u-b(U)]^2}u^{n+1}\mathrm{d}u\right) \\ &= \frac{2\lambda}{n+1}\langle u^{n+2}, g\rangle - \frac{2\lambda b(U)}{n+1}\langle u^{n+1}, g\rangle.\end{aligned}$$

Thus we get

$$\langle u^{n+2}, g\rangle = \frac{n+1}{2\lambda}\langle u^n, g\rangle + b(U)\langle u^{n+1}, g\rangle.$$

By the same procedure we may obtain

$$\langle u^{n+2}, g\rangle^\pm = \frac{n+1}{2\lambda}\langle u_n, g\rangle^\pm + b(U)\langle u^{n+1}, g\rangle^\pm.$$

In deriving the above properties, the following relations are useful:

$$\mathrm{erf}(x) = \frac{2}{\sqrt{\pi}}\int_0^x \mathrm{e}^{-u^2}\mathrm{d}u, \qquad \mathrm{erfc}(x) = 1 - \mathrm{erf}(x) = \frac{2}{\sqrt{\pi}}\int_x^\infty \mathrm{e}^{-u^2}\mathrm{d}u,$$

$$\mathrm{erf}(-x) = -\mathrm{erf}(x), \qquad \mathrm{erf}(0) = 0, \qquad \mathrm{erf}(\infty) = 1,$$
$$\mathrm{erfc}(0) = 0, \qquad \mathrm{erfc}(\infty) = 0.$$

APPENDIX II: THE CHAPMAN–ENSKOG EXPANSION OF THE BGK MODEL

The Chapman–Enskog expansion is a technique to obtain the deviation of a distribution function f from the equilibrium state g in terms of perturbations.[28,33] Consider a one-dimensional form of the BGK model:

$$\frac{\partial f}{\partial t} + u\frac{\partial f}{\partial x} = \frac{g-f}{\tau}.$$

The variables, including distribution functions, are non-dimensionalized by

$$\hat{x} = \frac{x}{l}, \qquad \hat{u} = \frac{u}{u_r}, \qquad \hat{t} = \frac{t}{l/u_r}, \qquad \hat{\tau} = \frac{\tau}{\tau_r}, \qquad \hat{f} = \frac{f}{f_r}, \qquad \hat{g} = \frac{g}{f_r},$$

where l, u_r, τ_r and f_r are a characteristic length, local reference speed, local reference collision time and local reference distribution function to make each term of order unity except for the small parameter $\hat{\epsilon}$. Then the original equation is non-dimensionalized as

$$\hat{\epsilon}\left(\frac{\partial \hat{f}}{\partial \hat{t}} + \hat{u}\frac{\partial \hat{f}}{\partial \hat{x}}\right) = \hat{g} - \hat{f}. \tag{33}$$

Now we may use a small parameter $\hat{\epsilon}$ to expand $\hat{f}$ as

$$\hat{f} = \hat{g} + \hat{\epsilon}\hat{g}_1 + \hat{\epsilon}^2\hat{g}_2 + \ldots = \sum_{n=0}^{\infty} \hat{\epsilon}^n \hat{g}_n, \tag{34}$$

where $\hat{g}_0 = \hat{g}$. Inserting equation (34) into equation (33), we get the recurrence relation

$$\hat{g}_n = -\left(\frac{\partial \hat{g}_{n+1}}{\partial \hat{t}} + \hat{u}\frac{\partial \hat{g}_{n+1}}{\partial \hat{x}}\right)$$

for $n \geqslant 1$. In the case $n = 1$ we get

$$\hat{f} \approx \hat{g} - \hat{\tau}\left(\frac{\partial \hat{g}}{\partial \hat{t}} + \hat{u}\frac{\partial \hat{g}}{\partial \hat{x}}\right). \tag{35}$$

If we apply equation (35) to thermodynamic systems of equations, we get the Navier–Stokes equations.

REFERENCES

1. J. P. Boris and D. L. Book, 'Flux corrected transport, 1 SHASTA, a fluid transport algorithm that works', *J. Comput. Phys.*, **11**, 38 (1973).
2. S. T. Zalesak, 'Fully multidimensional flux-corrected transport algorithms for fluids', *J. Comput. Phys.*, **31**, 335 (1979).
3. A. Harten, 'High resolution schems for hyperbolic conservation laws', *J. Comput. Phys.*, **49**, 357 (1983).
4. B. van Leer, 'Towards the ultimate conservative difference scheme. II, Monotonicity and conservatin combined in a second order scheme', *J. Comput. Phys.*, **14**, 361 (1974).
5. B. van Leer, 'Towards the ultimate conservative difference scheme. V. A second order sequel to Godunov's method', *J. Comput. Phys.*, **32**, 101 (1979).
6. A. Harten and S. Osher, 'Uniformly high-order accurate essentially non-oscillatory schemes. I', *SIAM J. Numer. Anal.*, **24**, 279 (1987).
7. A. Harten, B. Engquist, S. Osher and S. Chakravarthy, 'Uniformly high-order accurate essentially non-oscillatory schemes. III', *J. Comput. Phys.*, **71**, 231 (1987).
8. P. Colella and P. Woodward, 'The piecewise parabolic method(PPM) for gas-dynamical simulations', *J. Comput. Phys.*, **54**, 174 (1984).
9. P. Woodward and P. Colella, 'The numerical simulation of two dimensional fluid flow with strong shocks', *J. Comput. Phys.*, **54**, 115 (1988).
10. A. Jameson, 'Positive schemes and shock modelling for compressible flows', *Int. j. numer. methods eng.*, **20**, 743 (1995).

11. A. Jameson, 'Analysis and design of numerical schemes for gas dynamics 1. Artificial diffusion, upwind biasing, limiters and their effect on accuracy and multigrid convergence', *Int. J. Comput. Fluid Dyn.*, **4**, 171 (1995).
12. S. K. Godunov, 'A difference scheme for numerical computation of discontinuous solutions of hydrodynamic equations', *Math. Sborn.*, **47**, 271 (1959).
13. R. D. Richtmyer and K. W. Morton, *Difference Methods for Initial-Valued Problems*, Wiley, New York, 1967.
14. P. L. Roe, 'Approximate Riemann solvers, parameters vectors and difference schemes', *J. Comput. Phys.*, **43**, 357 (1981).
15. A. Harten, P. D. Lax and B. van Leer, 'On upstream differencing and Godunov-type schemes for hyperbolic conservation laws', *SIAM Rev.*, **25**, 35 (1983).
16. B. van Leer, 'Upwind-difference methods for aerodynamic problems governed by the Euler equations', in *Large-Scale Computations in Fluid Mechanics*, 1985.
17. P. L. Bhatnagar, E. P. Gross and M. Krook, 'A model for collision processes in gases. I. Small amplitude processes in charged and neutral one-component systems', *Phys. Rev.*l, **94**, 511 (1954).
18. R. Struijs, H. Deconinck, P. de Palma, P. L. Roe and K. G. Powell, 'Progress on multidimensional upwind Euler solvers for unstructured grids', *AIAA paper 91-1550*, 1991.
19. C. L. Rumsey, B. van Leer and P. L. Roe, 'A multidimensional flux function with applications to the Euler and Navier–Stokes equations', *J. Comput. Phys.*, **105**, 306 (1993).
20. J. C. Mandal and S. M. Deshpande, 'Kinetic flux vector splitting for Euler equations', *Comput. Fluids*, **23**, 447 (1994).
21. B. Perthame, 'Second-order Boltzmann schemes for compressible Euler equation in one and two space dimensions', *SIAM J. Numer. Anal.*, **29**, (1992).
22. W. M. Eppard and B. Grossman, 'A multi-dimensional kinetic-based upwind algorithm for Euler equations', *AIAA Paper 93-3303*, 1993.
23. K. H. Prendergast and K. Xu, 'Numerical hydrodynamics from gas-kinetic theory', *J. Comput. Phys.*, **109**, 53 (1993).
24. K. Xu and K. H. Prendergast, 'Numerical Navier–Stokes solutions from gas-kinetic theory', *J. Comput. Phys.*, **114**, 9 (1994).
25. K. Xu, L. Martinelli and A. Jameson, 'Gas-kinetic finite volume methods, flux-vector splitting and artificial diffusion', *J. Comput. Phys.*, **120**, 48 (1994).
26. K. Xu, C. Kim, L. Martinelli and A. Jameson, 'BGK-based schemes for the simulation of compressible flow', *Int. J. Comput. Fluid Dyn.*, **17**, 213 (1996).
27. R. J. Leveque, *Numerical Methods for Conservation Laws*, Birkhäuser, 1992.
28. M. N. Kogan, *Rarefied Gas Dynamics*, Plenum, New York, 1969.
29. E. S. Oran and J. P. Boris, *Numerical Simulation of Reacting Flows*, Elsevier, Amsterdam, 1987.
30. S. T. Zalesak, 'A preliminary comparison of modern shock-capturing schemes: linear advection', in *Advances in Computer Methods for Partial Differential Equations, VI, IMACS*, 1987, p. 15.
31. C. Hirsch, *The Numerical Computation of Internal and External Flows*, Vol. 2, Wiley, New York, 1990.
32. H. Q. Yang and A. J. Przekwas, 'A comparative study of advanced shock-capturing schemes applied to the Burgers' equation', *J. Comput. Phys.*, **102**, 139 (1992).
33. W. G. Vincenti and C. H. Kurger Jr., *Introduction to Physical Gas Dynamics*, Wiley, New York, 1967.
34. B. Einfeldt, 'On Godunov-type methods for gas dynamics', *SIAM J. Numer. Anal.*, **25**, 294 (1988).
35. P. L. Roe, 'Characteristic-based schemes for the Euler equations', *Ann. Rev. Fluid Mech.*, **18**, 337 (1986).
36. C. W. Shu, 'Efficient implementatin of essentially non-oscillatory shock capturing schemes, II', *J. Comput. Phys.*, **83**, 32 (1989).
37. P. K. Sweby, 'High resolution schemes using flux limiters for hyperbolic conservation laws', *SIAM J. Numer. Anal.*, **21**, 995 (1984).

